# FABRICATION OF HIGHLY TRANSPARENT INORGANIC/ORGANIC HYBRID MATERIALS AND THEIR APPLICATION AS TWO-PHOTON ABSORPTION MATERIALS

BY

YASUTAKA SUZUKI

# Contents

## Chapter 1 Introduction



## Chapter 2 Fabrication of Low Light-Scattering Inorganic/Organic Composites Suitable for Nonlinear Optical Measurements

# Chapter 3 Factors to Enhance Two-Photon Absorption Cross-Section of Organic Compounds by Hybridized with Inorganic Layered Compounds

# Acknowledgements

I take this opportunity to express profound respect and a deep sense of gratitude to *my guru*, Prof. Jun Kawamata. Without his constant guidance, encouragement and above all his cooperation, the thesis would not have taken this shape. I am indebted to him for the freedom he gave me in carrying out my research and the time he spent in trying to explain various facts and concepts. His commitment to the work with a great sense of dedication, motivation, discipline and patience are highly admirable and very inspiring.

I would like to thank the referees Professors Hitoshi Aoshima, Toshihiro Murafuji, Shoji Tagashira and Suzuko Yamazaki.

I am deeply indebted to all my teachers in school and college, especially Dr. Seiji Tani for their encouragement.

Thanks to Shoichiro Hirakawa, Maiko Fukudome, Ryuichi Seike, Takeshi Seno, Shinya Hasegawa, Nozomi Okawahara, Yuki Tanaka, Hiroshi Yamaki, Yu Furukawa, Takashi Maruyama, Tetsuo Ishigaki, Ryota Ohshige, Hiromasa Saito, Yusuke Sakamoto, Azumi Sumiyoshi, Ai Fujii, Chikako Ichimaru, Kenta Nakagawa, Daisuke Nakayama, Natsuki Matsuo, Ryoya Matsunaga, Akihiro Uchida, Junnya Kuroda, Honami Tarutani, Yuta Tenma, Takuya Honda, Kota Yamamoto, Yuki Kojima and Yukihiro Nishioka for making my lab life happy.

# Abstract

Two-photon absorption (TPA) is a phenomenon in which a material absorbs two photons simultaneously. The absorption rate of two-photon process increases quadratically with increasing excitation intensity. Therefore, by using a tightly focused laser beam as an excitation light source, a situation can be realized in which absorption occurs only at the focal point. In other words, three-dimensional (3D) spatial confinement in excitation can be realized by using the TPA process. TPA can therefore be utilized to perform 3D optical data storage, two-photon-excited fluorescence microscopy, 3D microfabrication, two-photon-induced photodynamic therapy, optical limiting, and so forth. However, the TPA cross-sections ($\sigma^{(2)}$), a value of the efficiency of TPA for one molecule, of known materials are too small for use in such applications. For TPA to occur in such materials, employment of an intense pulsed laser such as a femtosecond pulsed laser is required. On the other hand, materials with a large $\sigma^{(2)}$ enable two-photon excitation even when a common laser is employed as the light source. Therefore, development of materials with a large $\sigma^{(2)}$ is an important subject for study.

Organic materials intercalated in inorganic layered compounds often exhibit specific physical properties significantly different from those outside of the interlayer space. In fact, a preliminary study reported that the $\sigma^{(2)}$ of a dye intercalated in a clay mineral, which is a prototypical inorganic layered compound, at a specific condition is 10 times larger than that in solution. Thus, hybridization of organic dyes with a clay mineral has emerged as a promising means of obtaining efficient TPA materials. However, difficulties in fabricating such composites with negligible light-scattering and definite layer-by-layer stacking has prevented sufficient characterization of the optical properties of the dyes in the composites. Therefore, the reasons why the $\sigma^{(2)}$of the dye were enhanced in the composite are still not clear.

The first aim of this study is the establishment of a fabrication protocol for inorganic-layered-compound/dye composites that not only exhibit low light scattering but are also stacked definitely in a layer-by-layer manner The achievement of this aim will enable a comprehensive exploration of the spectroscopic characterization of such composites. The second purpose is the clarification of the reasons why the $\sigma^{(2)}$ of dyes were enhanced in the obtained composites compared to that in solution.

Chapter 2 describes a novel protocol established in this study for fabricating low light-scattering clay/dye composites by employing a clay mineral as a prototypical inorganic layered compound. When the sizes of the composite itself and the gap between the composite particles are sufficiently smaller than the wavelength of light, the incoherent light-scattering was considerably suppressed. This study has demonstrated that films, in which the clay/dye composites are densely packed so that the gap is smaller than the wavelength of light, can be

fabricated by optimizing the particle size of the clay, the concentration of the clay in dispersion and the amount of organics mixed with the dispersion. Based on this finding it has become possible to fabricate extremely low light-scattering composite films even when a variety of organic dyes and inorganic layered compounds were employed. As a result, reliable spectroscopic characterization of dyes in the composites has been enabled.

In Chapter 3, the reasons why the $\sigma^{(2)}$ of dyes were enhanced in the composite have been clarified. Several possible explanations of the enhanced TPA have been proposed. (1) Ionic interaction between the dye and the clay. (2) Improved molecular orientation results in the incident irradiation being more effectively utilized for excitation than in an isotropic system. This comes about, because, owing to the layer-by-layer stacking of the clay minerals parallel to the film plane, the $\pi$-plane of the molecules and the direction of electric field of incident light lie in the same plane when the films were irradiated by a laser beam propagating parallel to the normal direction of the film. (3) Improved planarity of the $\pi$-conjugated system of dyes induced by the intercalation. The contributions of these factors to the enhanced $\sigma^{(2)}$ were quantitatively investigated by employing four dyes as the guests. The results showed that the $\sigma^{(2)}$ of all the dyes intercalated in the clay films were enhanced because of reason (2) and occasionally due to (4), the hydrophobic environment of the interlayer space of clay minerals. The actual $\sigma^{(2)}$ of the dyes enhanced in these ways in the present films were two to three times larger than those in solution. A much more drastic enhancement of $\sigma^{(2)}$ was observed from dyes where planarity was improved on incorporation into the interlayer space of the clay mineral. For such dyes, not only the factors (2) and (4) were operating, but also factor (3), the extension of the $\pi$-conjugated system due to the improved planarity and the resulting factor (5), a decrease of detuning energy made substantial contributions to the enhancements of $\sigma^{(2)}$. In particular, the $\sigma^{(2)}$ of a porphyrin derivative in the film was found to be 13 times as large as that in solution. This clarification has enabled the design of efficient TPA materials based on inorganic-layered-compound/dye composites. This design strategy should be effective when other inorganic layered compounds than a clay mineral are employed.

It is worth mentioning that the features of the films obtained were suitable for TPA applications where a solid material is are required. One such is 3D optical-data storage, which is one of the most important applications of TPA materials because of the large commercial markets. The $\sigma^{(2)}$ of composites fabricated in this study were as large as that expected to be attained later than 2015 in the 2007 road-map of the Ministry of Economy, Trade and Industry. Thus it is concluded that the inorganic-layered-compound/dye composite film fabricated by employing the present film fabrication protocol should be a promising strategy for obtaining efficient TPA materials.

# Chapter 1 Introduction

## 1-1 Two-Photon Absorption

Two-photon absorption (TPA) is a phenomenon in which a material is excited by absorbing two photons. There are two types of TPA called resonant and nonresonant processes (Figure. 1-1).

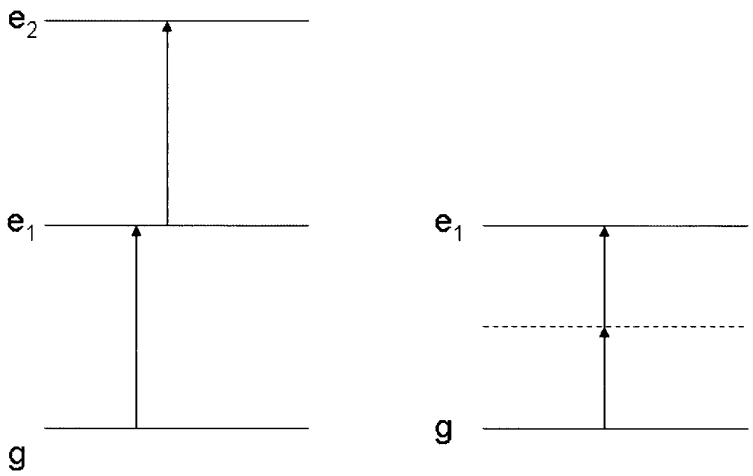


**Figure 1-1** Schematic representation of electron transition diagrams of resonant two-photon absorption (left) and nonresonant two-photon absorption (right). Here, g is the ground state and e refers to excited states.

The resonant TPA process (Figure 1-1, left) is also known as a cascade (stepwise) TPA process. The first photon is used for excitation from the ground state (g) to an excited state ($e_1$). Then the material system absorbs a second photon and is excited to a higher excited state ($e_2$). Theoretically, the absorption rate of the resonant two-photon process increases quadratically with increasing excitation intensity, when the intensity of incident beam is relatively low. However, the absorption rate of the process increases linearly with increasing excitation intensity[1] when the material system is intensely excited.

The nonresonant TPA process (Figure 1-1 right) is a phenomenon in which a material absorbs two photons simultaneously. The broken line shown in Figure 1-1 right represents not a real state, but a virtual intermediate state similar to the case of Raman scattering. The absorption rate of a

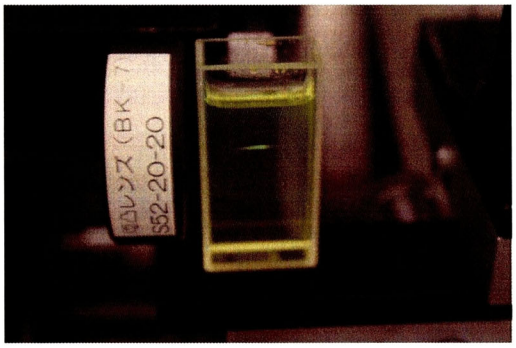


**Figure 1-2** Photograph of TPA induced fluorescence from an ethanol solution of 1,1'-diethyl-4,4'-(9,9-diethyl-2,7-fluorenediyl-2,1-ethenediyl)dipyridinium perchlorate irradiated by a tightly focused femtosecond pulsed laser beam at a wavelength of 820 nm.

non-resonant two-photon process always increases quadratically with increasing excitation intensity.

The transition probability of a nonresonant two-photon process was first derived by Maria Göeppert-Mayer, in 1931, using second-order perturbation theory[2]. Recognizing her foresight, an informal unit (GM, the name abbreviation of Göeppert-Mayer, 1 GM is defined by $1.0\times10^{-50}$ $cm^4$ s $photon^{-1}$ $molecule^{-1}$) is often used as the unit of nonresonant molecular TPA cross-section ($\sigma^{(2)}$), which is a value of the efficiency of nonresonant TPA of one molecule. The first experimental observation of nonresonant TPA was in 1961, 1 year after the invention of the first laser device. W. Kaiser and C. G. B. Garrett reported a TPA induced frequency-upconversion fluorescence in a $CaF_2:Eu^{2+}$ crystal sample, excited by the intense coherent radiation of 694.3 nm wavelength from a pulsed ruby-crystal laser[3]. Since then, nonresonant two- and multi-photon processes have developed into a major new research area for exploration by scientists and engineers.

Since the absorption rate of nonresonant two-photon process always increases quadratically with increasing excitation intensity, by using a tightly focused laser beam as an excitation light source, a situation can be realized in which absorption occurs only at the focus point. Figure 1-2 shows fluorescence emission from the solution of a fluorophore irradiated by a focused femtosecond pulsed beam at a wavelength of 820 nm. A TPA induced frequency-upconversion green fluorescence

emission can be seen only at the center of the cell, namely the focal point. Thus, spatial selective excitation can be realized by utilizing the quadratic dependence of light absorption of the nonresonant TPA. The spatial selectivity of excitation of nonresonant TPA can therefore be utilized to perform 3D optical data storage[4-13], 3D microfabrication[14-18], two-photon excited cell imaging[19-23], photodynamic therapy [24-26] and so forth. Also, the quadratic dependence of light absorption of the nonresonant TPA is expected to realize optical limiting[28-31].

Since various applications are expected for nonresonant TPA, it is often simply called TPA. Therefore, in this paper, the term TPA is hereafter used as a short form for nonresonant TPA.

## 1-2 Applications of Two-Photon Absorption

### 1-2-1 Three-Dimensional Optical Data Storage[4-13]

As a promising high-capacity memory alternative to compact disc-recordable (CD-R) or digital versatile disc-recordable (DVD-R), high density three-dimensional (3D) optical data storage making use of theTPA phenomena is attracted increasing interest. Promising means of 3D optical data storage are 3D bit optical data recording[4-12] and holographic memory[13]. The 3D bit optical data recording is categorized into the two-photon[4-9], the simple multi-layered[10], the electrically-layer-selective[11] and 3D holographic stamping[12] types. Among these types, the two-photon recording type is most attractive because of the durability of current optical memories, such as DVD and Blu-ray, and existing technologies.

In the two-photon recording type of 3D optical data storage, the 3D bit pattern is recorded by utilizing the high spatial selectivity of TPA. Several prototypical media consisting of alternative stackings of recording and buffer layers as represented in Figure 1-3 have been fabricated. The buffer layer plays an important role to suppress cross talk between the recording layers. The layer to be recorded can easily be selected by moving the lens and thus the depth of the focal point. Most of the existing systems utilize heat-mode recording, where the light is converted into thermal energy, which induces a magnetic or structural phase transition (magneto-optical and phase-change effects)

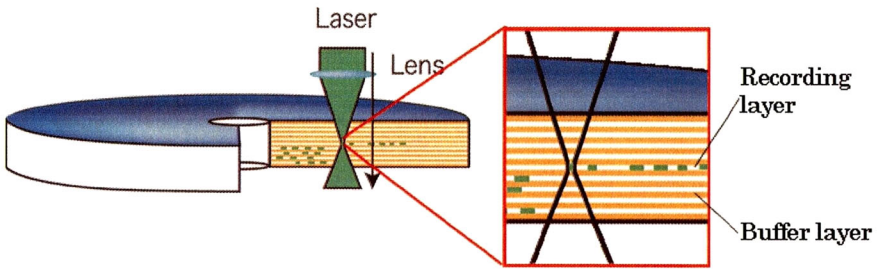


**Figure 1-3** Schematic representation of a prototypical two-photon recording type 3D optical data storage medium.

and changes the physical properties of the medium. In the photon-mode of data recording, the light initiates a photochemical reaction of a particular component of the material.

Progress in drive technology has made it possible to provide several experimental two-photon recording type optical drives mountable in conventional tower-type personal computers. However, the $\sigma^{(2)}$ of known materials are too small. For TPA to occur in such media, the employment of an intense pulsed laser such as a femtosecond pulsed laser is required. Therefore, materials with large $\sigma^{(2)}$ which enables two-photon excitation even when a common laser is employed as the light source are strongly desired.

## 1-2-2 3D Micro-Fabrication[14-18]

The features of high spatial confinement of multiphoton interactions and the penetrating capability of a focused laser beam can be used to create 3D microstructures to fabricate micromachines with subdiffraction-limit spatial resolution[14-18]. This technique is essentially a multiphoton-interaction-based 3D photolithography. By using this technique, various micromachines, as exemplified in Figure 1-5, such as photonic crystals, optical waveguides, rotors and so forth, have been fabricated.

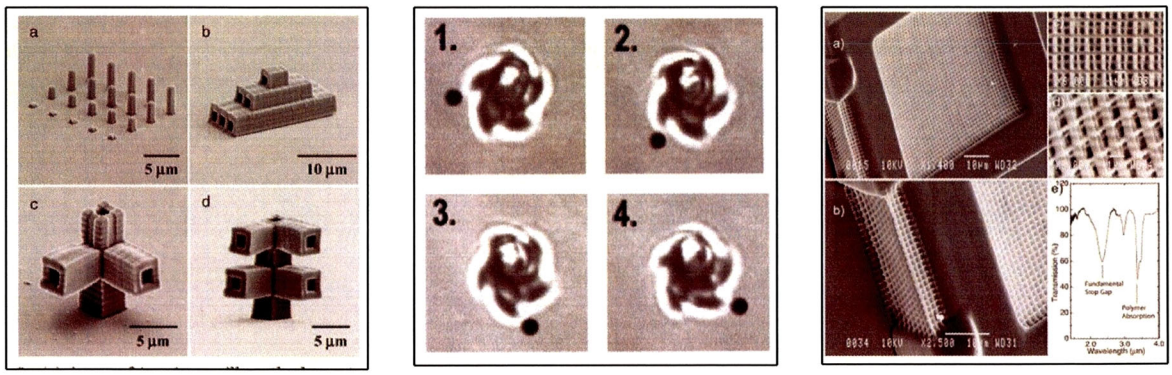


**Figure 1-5** Examples of micromachines fabricated by two-photon excitation based 3D photolithography. Left: microcapillary (C. A. Coenjarts et al.[15]), center: rotor (P. Galajda et al.[16]), right: woodpile structured photonic crystal (L. H. Nguyen et al.[17]).

## 1-2-3 Two-Photon Induced Fluorescence Imaging[19-23]

Fluorescence imaging is used to study the properties of organic or inorganic substances using the phenomena of fluorescence and phosphorescence. Especially, this technique is widely used in biological fields. In most cases, a component of interest in the specimen can be labeled specifically with a fluorescent molecule. The specimen is then illuminated with light of a specific wavelength which is absorbed by the fluorophores, causing them to emit light of longer wavelengths. By observing the emitted light, the location of the component can be specified.

Two-photon induced fluorescence microscopy is a fluorescence imaging technique that utilizes two-photon excitation instead of one-photon excitation[19-23]. Compared to conventional optical microscopy, two-photon excited fluorescence microscopy has a number of advantages, with the first being the inherent 3D localization of excitation and fluorescence arising from the quadratic dependence on the input intensity. This quadratic or nonlinear dependence limits excitation to a tiny focal volume, which restricts both out-of-focus background excitation and provides intrinsic confocality, since only fluorophores in the plane of the focused beam will be excited. This removess the need for a confocal aperture in front of the detector, thus maximizing the amount of light detected. Second, two-photon excited fluorescence microscopy often utilizes the near-infrared spectral window, so the imaging depth is much greater and scattering is reduced, resulting in less

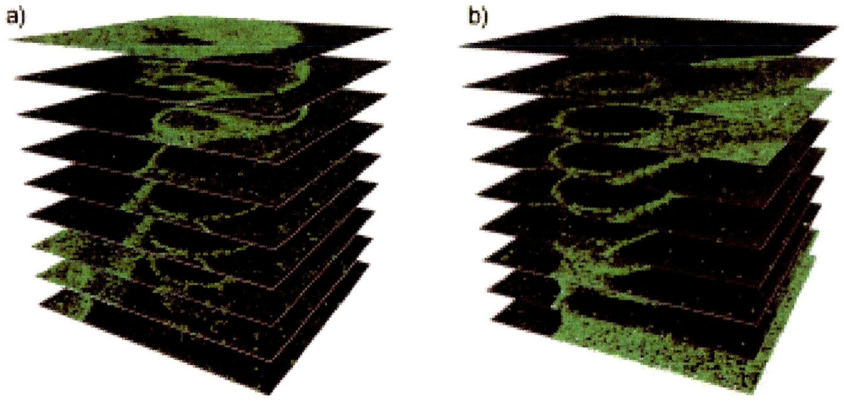


**Figure 1-4** Example of two-photon absorption imaging[23]; optical sections of lamin proteins in the nucleus of a human glioma cell imaged by using two-photon absorption with 747 nm excitation.

photodamage and photobleaching than that caused by a one-photon excited fluorescence techniques. In addition, higher signal-to-background ratios for fluorescence detection are possible resulting from the well-separated excitation and emission wavelengths and reduced attenuation of near-infrared light in biological specimens relative to UV and visible wavelengths. Two-photon induced fluorescence microscopic images provided in reference 23 are shown in Figure 1-4.

Fluorophores commonly used for two-photon induced fluorescence microscopy in biological fields are rhodamine derivatives and a series of Green Fluorescence Proteins (GFP). The $\sigma^{(2)}$ of the former is about 200 and that of the latter is only few GM. Therefore, an intense light source such as femtosecond pulsed laser is also typically required for two-photon excitation microscopy. If a fluorophore with a large $\sigma^{(2)}$ can be obtained, high-sensitivity and low-damage 3D imaging can be realized. Therefore, exploration of an efficient TPA dye suitable to the two-photon induced fluorescence microscopy is important for extending the applicability of the microscope technique.

### 1-2-4 Two-Photon Photodynamic Therapy[24-26]

The benefits that TPA brings to microscopy also translate to photodynamic therapy (PDT). One-photon PDT[27] is widely used to treat cancers of the skin and hollow organs, as well as the eye disease macular degeneration. PDT employs a photosensitizer, which is harmless in the absence of light, to induce damage upon optical irradiation. The phototoxicity of these photosensitizers is primarily due to singlet oxygen, which is generated by energy transfer from the excited state of the sensitizer to molecular oxygen. Two-photon PDT[24-26] should confine excitation of the photosensitizer to the focal volume. The longer-wavelength (near-IR) light required for two-photon excitation also penetrates deeper into living tissues than visible light. These advantages make TPA PDT of particular interest in neurology and ophthalmology, where there is a need to improve

therapeutic targeting whilst simultaneously minimizing invasiveness.

The small TPA cross-sections of the drugs typically used (<100 GM) has necessitated the use of laser powers close to the tissue-damage threshold. Hence, two-photon PDT with these sensitizers is impractical as a clinical treatment: the cumulative effect of scanning the focus through the disease volume would cause indiscriminate photodamage. New photosensitizers with high $\sigma^{(2)}$ values are needed to allow a significant reduction in irradiation intensities and treatment times, and make TPA PDT an attractive therapeutic strategy.

### 1-2-5 Optical Power Limiting[28-31]

An optical limiter, utilizing the quadratic dependence of absorption rate of two-photon process on excitation intensity, is an important application[28-31]. Optical limiters have been utilized in a variety of circumstances where a decreasing transmission with increasing excitation is desirable. For example, these devices have been used for various laser pulse shaping applications. While saturatable absorbers had long been used for pulse compression, Q switching and mode locking, in 1984 Harter and Band[29] demonstrated that an optical limiter consisting of a reverse saturatable absorber could be used for passive mode locking. Harter et al.[30] have also shown that amplitude modulated pulses can be smoothed by an optical limiter, provided that the duration of the amplitude substructure is long compared to the activation time of the limiter. In this application, a long optical pulse with short intensity spikes incident on the limiter will have the spikes preferentially attenuated with respect to the average pulse shape. Eye protection from an intense laser beam is also expected as a future application of an optical limiter.

### 1-2-6 Requirements for Realizing Applications of Two-Photon Absorption

As described above, the applications of TPA are still not widely utilized, though the use of

two-photon excitation possesses various merits. This is because, so far, the use of an intense and expensive pulsed laser such as a femtosecond pulsed laser is required to take advantage of the TPA occurring in known materials. In order to widely utilize the merits of TPA in related applications, the development of both compact and cheap intense pulsed lasers and materials with large $\sigma^{(2)}$ are urgently required.

## 1-3 Efficient Two-Photon Absorption Materials

TPA of molecular materials is attractive due to their efficient and high speed responses compared to those of inorganic materials. Therefore, interests in the development of efficient TPA materials have been mainly focused on molecular materials. Here, based on the three-state model, let us theoretically consider how efficient TPA materials should be designed. According to perturbation expansion theory[32,33], $\sigma^{(2)}$ at the lowest energy TPA transition ($\sigma^{(2)}_{peak}$) can be written as:

$$\sigma^{(2)}_{peak} \propto \frac{\left|\mu_{kg}\right|^2 \left|\mu_{e_1 k}\right|^2}{\Delta E^2 \Gamma_{e_1 g}} E^2_{e_1 g}$$

where $\mu_{kg}$ is the transition dipole moment from the ground state ($g$) to the lowest one-photon absorption (OPA) allowed energy level ($k$), $\mu_{e_1 k}$ is the transition dipole moment from $k$ to the lowest TPA allowed energy level ($e_1$), $E_{e_1 g}$ is the energy gap between $g$ and $e_1$, $\Delta E$ (i.e., the detuning energy) is the difference between the energy of the photon used for two-photon excitation and the energy gap between $g$ and $k$ ($\Delta E = (E_{kg} - \frac{1}{2}E_{e_1 g})$) and $\Gamma_{e_1 g}$ is a damping factor.

Up to now, strategies for the design efficient TPA materials have focused on obtaining molecules with large transition moments . This is largely because the transition moments of molecules can be estimated by means of molecular-orbital calculation techniques. The oscillator strength is proportional to the square of the transition dipole moment[34]. Thus, molecules with large $\sigma^{(2)}_{peak}$ can be found from those exhibiting large transition dipole moments. Several studies have increased the transition dipole moments by extending π-conjugated systems[33,35-39]. In addition, an effective and widely used strategy for enhancing the transition dipole moment is to introduce electron donor (D) and acceptor (A) groups at the ends of $p$-conjugated systems[40-61]. For example, the $\sigma^{(2)}_{peak}$ of compound (b) in Figure 1-6, 210 GM , was reported to be about 18 times greater than that of $E$-stilbene (Figure 1-6 (a))[39]. This large $\sigma^{(2)}_{peak}$ of (b) compared to (a) has been attributed to the

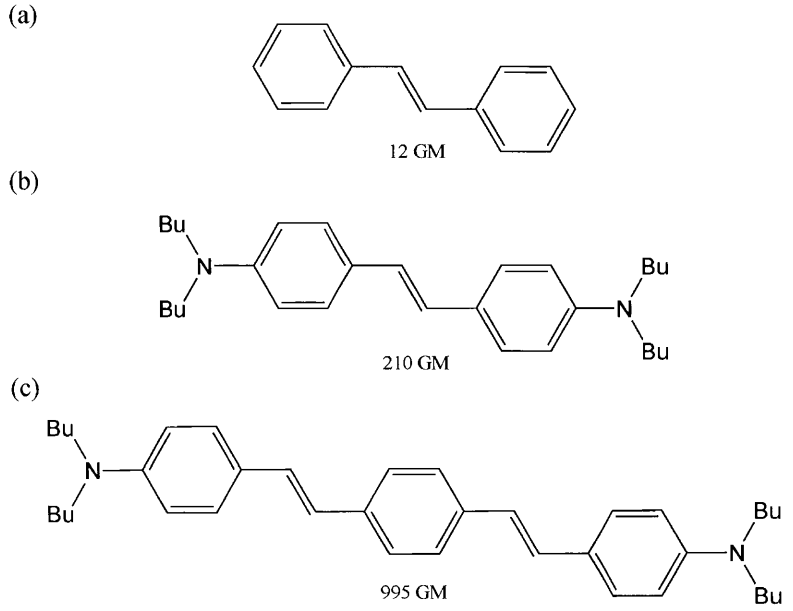


**Figure 1-6** Example of enhancement of $\sigma^{(2)}_{peak}$ by extension of π-conjugated systems and introduction of electron donor groups[39]

introduction of strong donor groups at the both ends of the π-electron system. The $s^{(2)}_{peak}$ of compound (c) in the same figure (ca. 995 GM) was reported to be 5 times larger than that of compound (b)[39]. This is due to the further extension of the π-electron system.

Improvements of planarity of the π-electron system is known to enhance delocalization of π-electron system and thus obtain large a $\sigma^{(2)}_{peak}$[40]. This can be seen from a comparison of $s^{(2)}_{peak}$ values of the compounds shown in Figure 1-7 (a) and (b). Although the backbones of the π-electron systems of both compounds are the same, the former, which is equipped with a five-membered central ring, possesses an almost planar π-electron system, whereas the seven-membered central ring of the latter results in considerable distortion of the π-electron system. Because of the difference of the planarity in the π-electron systems, the $\sigma^{(2)}_{peak}$ of the former is 960 GM whereas the value of the latter is 140 GM[40]. This difference clearly indicates the planarity of π-electron system considerably influences TPA efficiency.

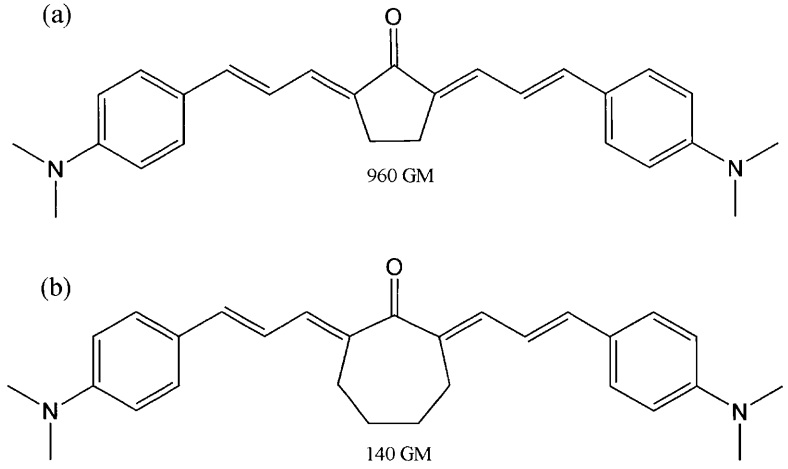


**Figure 1-7** TPA cross-sections of molecules with planar (a) and distorted π-electron systems (b)[40].

It is reported that the $\sigma^{(2)}_{peak}$ of D-π-A-π-D[40,41,44,46,48,50,51,54] and A-π-D-π-A[43,51,53,55] type compounds are larger than those of D-π-A[41-50], D-π-D[45,46,51,52] and A-π-A[43,53] type compounds. As shown in Figure 1-8, the $\sigma^{(2)}_{peak}$ of D-π-A (a)[41] and D-π-D (b)[42] compounds are 140 and 50 GM, respectively, whereas the value of a D-π-A-π-D compound (c)[41] is 960 GM. The magnitude of (c) is 7 times as large as that of compound (a) and 19 times as large as that of compound (b). Similarly, the $\sigma^{(2)}_{peak}$ of an A-π-D-π-A compound[43] (e), 848 GM is 2.3 times as large as that of a A-π-A compound[43] (d) of 363 GM.

Based on the above mentioned strategies for enhancing the transition moments of molecules, several compounds exhibiting very large $\sigma^{(2)}_{peak}$ values of over than 10000 GM have been designed[56-59]. However, it is not practical to design compounds exhibiting even larger $\sigma^{(2)}_{peak}$ values only by enhancing transition moments. This is because it is difficult for molecules possessing large number of π-electrons to maintain the planarity of the π-electron system over the whole molecule. Therefore, there is a limit in the possible enhancement of $\sigma^{(2)}_{peak}$ by extending the π-electron system. For example, in macrocyclic thiophene *n*-mers (Figure 1-9), the absolute values of $\sigma^{(2)}_{peak}$ increase across the series, but the value of $\sigma^{(2)}_{peak}$ normalized by the number of π-electrons ($\sigma/N_e$) saturates with increasing linker size as shown in Figure 1-9. In addition, there are several additional problems,

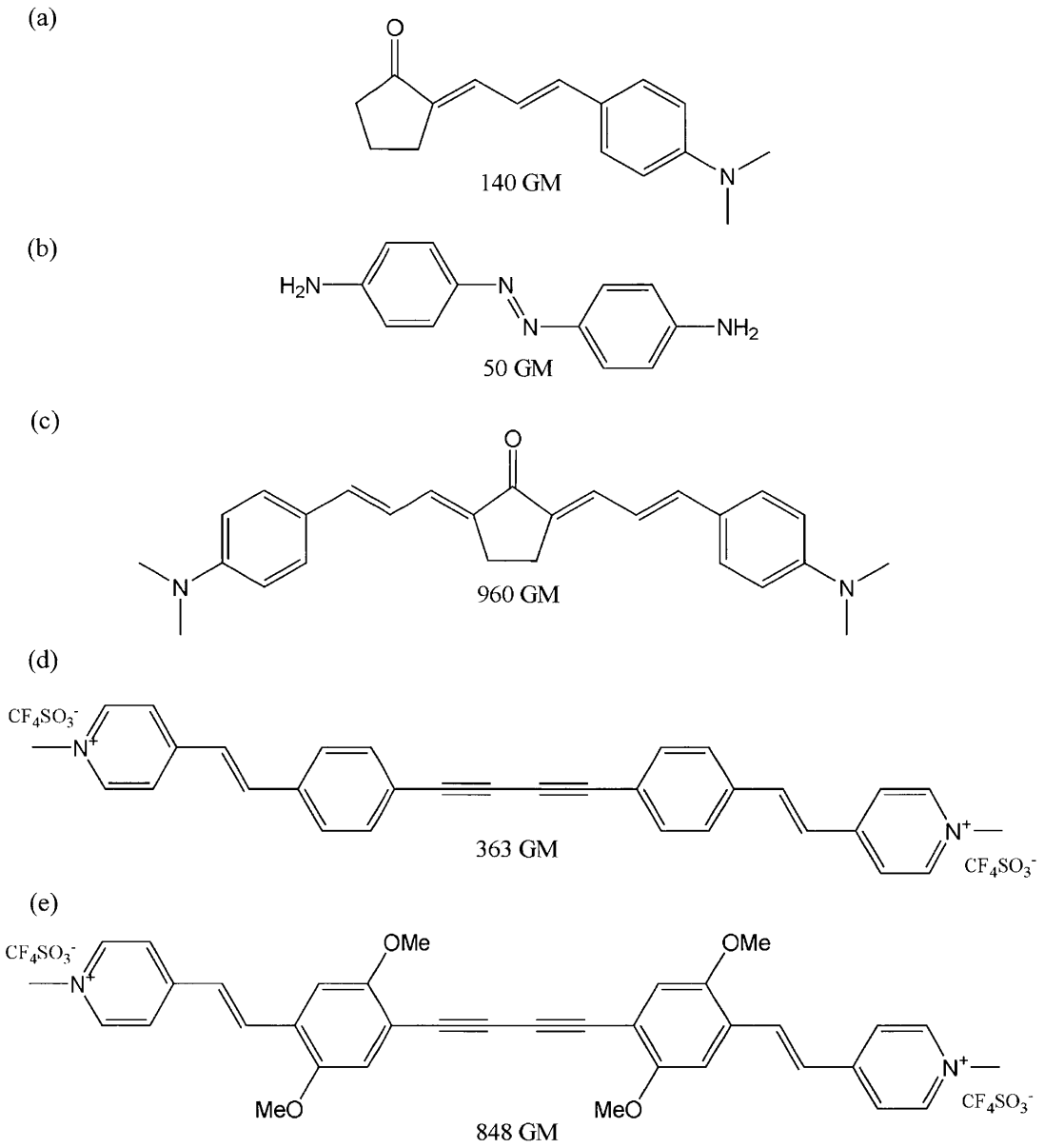


**Figure 1-8** Differences in $\sigma^{(2)}_{peak}$ values for D–π–A[41], D–π–D[42], D–π–A–π–D[41], A–π–A[43] and A–π–D–π–A[43] type compounds

such as low solubility and tedious synthesis, which hinder the practical application of compounds possessing very large π-electron systems. Therefore, in order to obtain TPA materials exhibiting larger values of $\sigma^{(2)}_{peak}$, alternative design strategies other than the enhancement of transition moments are definitely required.

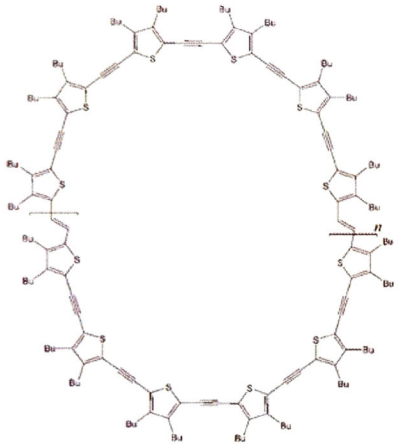

| $n$ | $\sigma^{(2)}_{peak}$ (GM) |
|---|---|
| 1 | 15000 |
| 2 | 67000 |
| 3 | 83000 |
| 4 | 110000 |

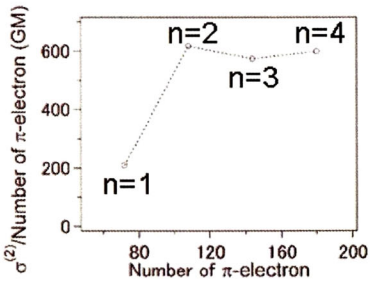


**Figure 1-9** Values of $\sigma^{(2)}$ of macrocyclic thiophene $n$-mers as a function of $n$[60].

Several attempts have been made to design molecules with a small $\Delta E$ as an alternative strategy. A schematic representation of the energy diagram of a typical organic dye is shown in Figure 1-10(a). In most cases, the lowest TPA-allowed state is located near the lowest OPA allowed state. Therefore, the magnitudes of $\Delta E$ of typical dyes are almost the same as the photon energy used for TPA excitation. The value of $\Delta E$ is small when the difference between the energy of a single photon for two-photon excitation and the energy of an OPA allowed excitation is small. Therefore, a specific molecule having the energy diagram shown in Figure 1-10 (b) will have a small $\Delta E$. To intentionally create such a situation, independent control of a TPA-allowed energy level and/or an OPA-allowed energy level is required. However, no such method has yet been established. Consequently, no molecular design strategy for deliberate tuning of the $\Delta E$ has been proposed.

To effectively reduce $\Delta E$, the use of a TPA transition to a higher excited state that is located at almost twice the energy of the lowest OPA allowed excited state (often called the double resonance transition) has been investigated[44]. This transition can occur in a molecule possessing the energy diagram shown in Figure 1-10 (c). This is an attractive strategy for reducing $\Delta E$; however, there is no effective strategy for designing a molecule with such an energy diagram.

Hirakawa et. al. proposed another unique strategy in 2008[60]. Rather than attempting $\Delta E$ tuning,

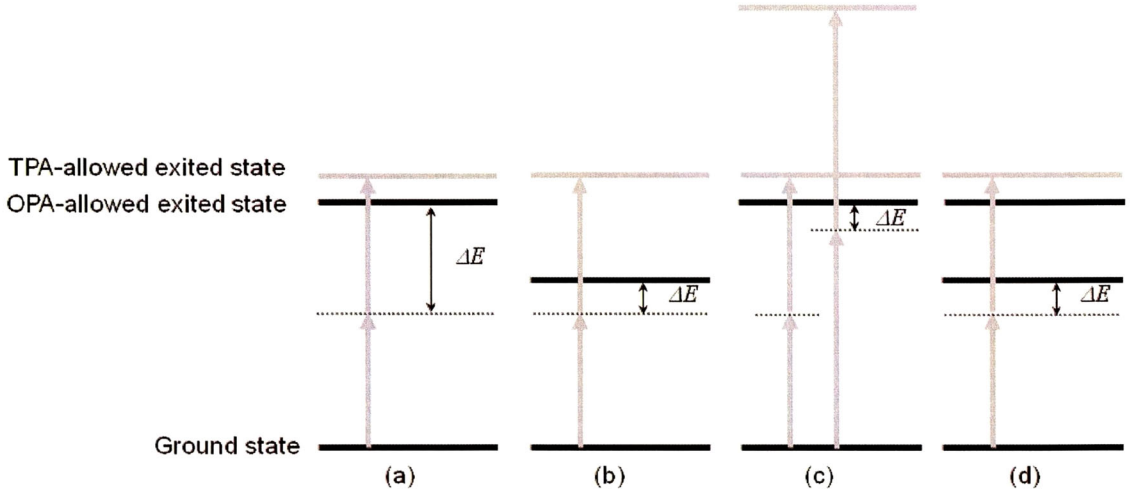


**Figure 1-10** Schematic representation of energy diagrams of a typical organic dye (a) and dyes with a small detuning energy (b)-(d). Bottom line represents ground state. Black lines and gray lines represent OPA- and TPA-allowed excited states, respectively.

they explored molecules having similar energy diagrams to that shown in Figure 1-10 (d). As shown in Figure 1-11, azulene exhibits an interesting spectroscopic property: its main absorption band is assigned to the transition from the ground state ($S_0$) to the second one-photon excited state ($S_2$). Because $S_1$ is located almost halfway between $S_2$ and $S_0$, the electronic features specific to azulene are suitable for obtaining a small $\Delta E$ with regard to the $S_2$-related TPA transition. Unsubstituted azulene must have a small $\sigma^{(2)}$ value because its π-electron system is considerably smaller than those of efficient TPA chromophores. However, this drawback can be overcome by incorporating an azulenyl moiety in a large planar π-electron system. This provides a large transition moment in addition to a small $\Delta E$ for the azulenyl groups, so that excellent TPA properties are expected. To obtain efficient nonlinear optical compounds, a series of derivatives having azulenyl group(s) at the end(s) of favorable ketone backbones, sucn as ethylidenecyclopentanone or bis(ethylidene)cyclopentanone, have been designed. Figure 1-12 (a) shows the chemical structures of the azulene derivative, α,α'-bis(1-azulenylidene)cyclopentanone, designed using this principle. The structure of the benzenoid structural isomer, α,α'-di(1-naphtylidene)cyclopentanone, is also shown in Figure 1-12 (b). The $\sigma^{(2)}{}_{peak}$ of (a) (270 GM) was 7 times larger than that of (b) (40 GM), even

though (a) is a structural isomer of (b)[60]. Thus, introducing a substituent that has specific electronic characteristics, such as an azulenyl group, is an effective means for obtaining an organic compound with a small $\Delta E$, thereby resulting in a large $\sigma^{(2)}_{peak}$. However, limited numbers of compounds exhibit such electronic properties. Furthermore, syntheses of such compounds are not easy. Thus, the strategy proposed by Hirakawa et. al. still has limitations.

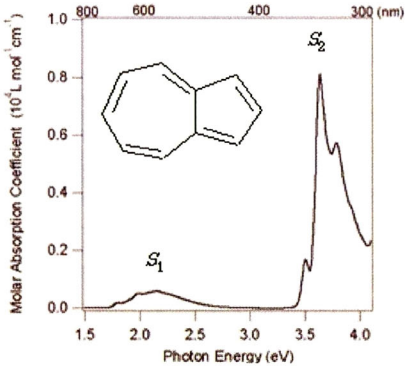


**Figure 1-11** Chemical structure and one-photon absorption spectrum of azulene.

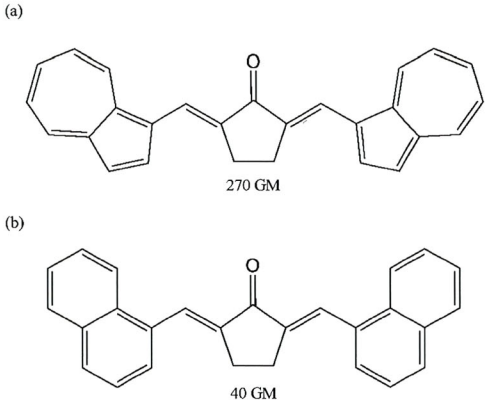


**Figure 1-12** Comparison of $\sigma^{(2)}_{peak}$ values of an azulenyl compound (a) and the benzenoid structural isomer (b)[60].

## 1-4 Inorganic Layered Compounds and their Hybrid Materials with Photo-Functional Dyes

### 1-4-1 Inorganic Layered Compounds: Clay Minerals[61]

Clay minerals are the prototypical inorganic layered compound. The structure of saponite, one of the most typical clay minerals, is shown in Figure 1-13. Clay minerals possess a layered structure due to the space produced by condensation of an octahedral $Al_2O_3$ or MgO planar sheet between two planar tetrahedral $SiO_2$ sheets, the so-called 2:1 layer structure. Most inorganic layered compounds, including clay minerals, have a negative charge. For example, in the case of clay minerals, isomorphic substitution of tetrahedral $Si^{4+}$ (tetrahedral substitution) and/or octahedral substitution of $Al^{3+}$ or $Mg^{2+}$ (octahedral substitution) by other metals with lower valence result in a negative layer charge. The negative charges are compensated by exchangeable inorganic cations which are commonly hydrated and are located on the surface of the layers. Through the electrostatic attractive force between clay layers and the exchangeable metal cations, the clay layers form a layer-by-layer stacking structure. The clay minerals have the ability to show extensive interlayer swelling in water; under optimum conditions, the layers can completely dissociate (delaminate). The interlayer cation can easily be exchanged by other cations, including organic cations, in aqueous dispersion. The propensity of clay mineral for sorbing cationic species from solution is experessed as the cation exchange capacity (CEC). CEC values are expressed in centimole of positive charge per kilogram of dry clay mineral (mol(+)/kg) which is numerically equal to the traditional unit of milliequivalents per g clay (meq/g). The cationic dye content of a clay/dye system is generally expressed as a percentage of the CEC of the clay (% CEC).

Typical clay minerals possessing the 2:1 layer structure are saponite and montmorillonite. The difference between them is the valence of the metal ions occupied in the center of the octahedron, being trivalent and divalent, respectively. This valence difference results in the different structures of

the octahedral sheets. When the octahedrons are composed of trivalent and divalent cations, structures referred to as dioctahedral (Figure 1-14 (a)) and trioctahedral (Figure 1-14(b)) sheets are respectively formed[62].

In this thesis, the terms "hybridization" and "composite" are defined as "hybridization of cationic organic compounds with inorganic layered compounds through the ion-exchange reaction" and "the resulting hybrid particle consisting of the cationic organic compounds and inorganic layered compounds", respectively.

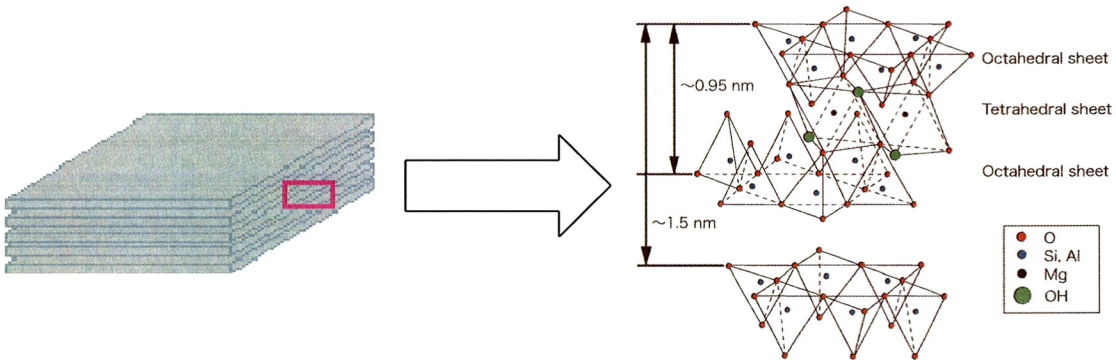


**Figure 1-13** Crystal structure of saponite. Schematic representation of layer-by-layer stacking of clay layers is also shown (left).

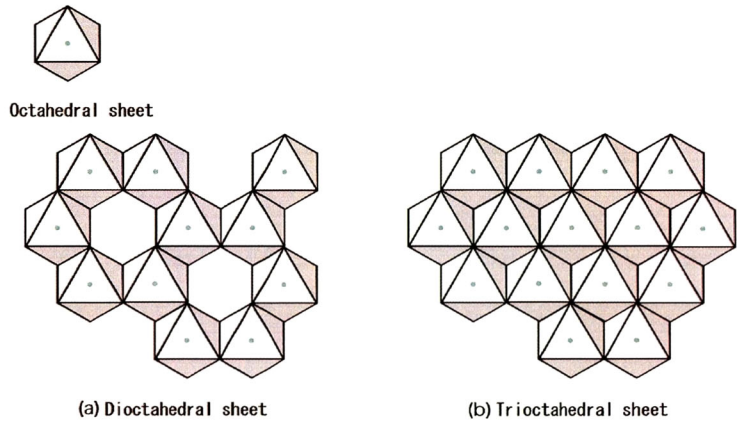


**Figure 1-14** Di- (left) and tri- (right) octahedral structures of the inner sheet of clay layers.

## 1-4-2 Electronic properties of clay/dye composites

Clay minerals do not absorb light in the visible wavelength region. Therefore, in the last two decades, various composites consisting of clay minerals and photo-functional organic compounds have attracted considerable interest. For example, Sasai et.al. reported that concentration quenching of fluorophores intercalated in the interlayer space of clay minerals is effectively suppressed even at a quite high density[63,64] (see Figure 1-15). Takagi et. al. demonstrated that the alignments, orientation and intermolecular distances of molecules adsorbed on clay minerals are controllable and thus unique electron- or energy transfer systems can be constructed[65,66] (see figure 1-16).

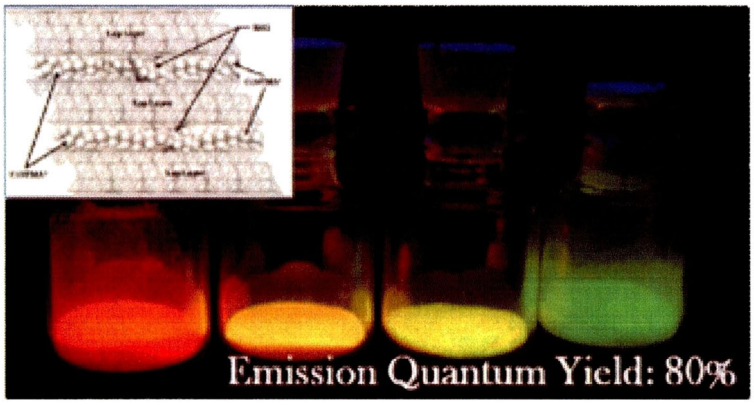


**Figure 1-15** Intense concentration quenching free fluorescence from clay/dye composites demonstrated by Sasai, et. al. Copied from http://www.phys.shimane-u.ac.jp/ryo_lab/ with permission.

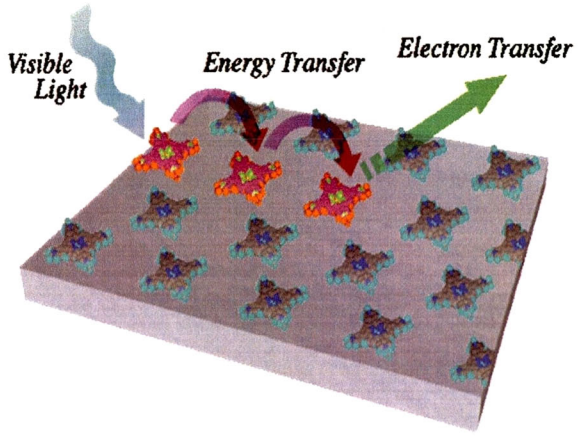


**Figure 1-16** A model of an artificial light harvesting (electron- and energy-transfer) system composed of a clay/porphyrin composite demonstrated by Takagi, et al. Copied from http://www.apchem.ues.tmu.ac.jp/labs/takagi/research.html with permission.

Hybridization of organic dyes with a clay mineral has emerged as a promising means of obtaining efficient TPA materials. Kamada et al. reported the value of $\sigma^{(2)}_{peak}$, that is, the probability of TPA per one molecule, of 1,4-bis(2,5-dimethoxy-4-{2-[4-(*N*-methyl)pyridinium]ethenyl}phenyl)-butadiyne triflate (MPPBT, Figure 1-17) in a hybrid film consisting of MPPBT and a synthetic saponite (Smecton SA (SSA)) at 20% CEC was 2.5 times the value measured in dimethylsulfoxide (DMSO) without clay[67]. However, in order to utilize clay/dye composites as TPA materials, two problems should be addressed. First, conventional clay/dye composites are strong light-scattering media. This incoherent light-scattering prevents not only use of the composites as optical materials but also hinders effective characterization of the optical properties of dyes in the composite. In such circumstances, the reasons why $\sigma^{(2)}_{peak}$ of MPPBT was enhanced in the composite are still not clear. It is reported that the $\sigma^{(2)}_{peak}$ of MPPBT-SSA composites at 800 nm showed considerable dependence on the %CEC[68]. Furthermore, significant enhancement of $\sigma^{(2)}_{peak}$ was not observed when other dyes than MPPBT were intercalated into a clay mineral[69].

## 1-5 Purpose and Outline of This Work

As for the reasons why $\sigma^{(2)}_{peak}$ of MPPBT were enhanced in the composite, so far, the following three possibilities have been proposed[67].

(1)Substitution of the counter anion of the dye obtained by adsorption onto the clay through an ion-exchange reaction.

(2)Improved molecular orientation of dyes. In composite films, the orientation of dyes should be confined owing to the oriented stacking of the two-dimensional clay layers. Therefore, the incident irradiation should be more effectively utilized for excitation than in an isotropic system when the π-plane of the molecules and the direction of the electric field of the incident light lies in the same plane if the films are irradiated by a laser beam propagating parallel to the normal direction of the film.

(3)Extension of the π-conjugated system due to the improved planarity obtained by the confinement of the chromophore in the 2-dimensional nanospace formed between the clay layers.

Fabrication of low light-scattering clay/dye mineral composites with a definite layer-by-layer stacking mode of composites enables valuable investigations of changes in electronic properties and molecular orientation of dyes accompaning the hybridization with clay minerals. The results should give the answer to the question: why $\sigma^{(2)}_{peak}$ of dyes were enhanced in the composite. The answer should enables the design of clay/dye composites exhibiting enhanced $\sigma^{(2)}_{peak}$. In other words, a novel design principle of efficient TPA materials should be established.

Chapter 2 describes a novel protocol for fabricating low light-scattering inorganic-layered-compound/dye composites established in this study. When the sizes of the composite itself and the gap between the composite components are sufficiently small compared to the wavelength of the light, incoherent light-scattering should be considerably suppressed. This study has demonstrated that films in which the clay/dye composites are densely packed so that the

gap is smaller than the wavelength of light, can be fabricated by optimizing the particle size of the clay, the concentration of the clay in the dispersion and the amount of organics mixed with the dispersion. Based on this finding it has become possible to fabricate extremely low light-scattering composite films even when a variety of organic dyes and inorganic layered compounds were employed. Furthermore, in the composite films, the clay/dye composites were found to be stacked in a definite layer-by-layer manner. As a result, reliable spectroscopic characterization of dyes in the composites has been possible.

In Chapter 3, the reasons why the $\sigma^{(2)}_{peak}$ of MPPBT were enhanced in the composite have been clarified by employing a clay mineral as the host. Tarutani et. al. recently reported that the factor (1), the difference in the counter anion of the dye, does not make any obvious contribution to TPA properties[70]. Among the remaining two previously proposed factors expected to enhance the $\sigma^{(2)}_{peak}$ of dyes in the composite films, the effect resulting from the improved molecular orientation of chromophores in between the clay layers (2) should be observed in all of the clay/dye films fabricated by the protocol, because the composites are definitely stacked layer-by-layer in the film. On the other hand, for composites consisting of dyes of which planarity should be improved by intercalation, such as MPPBT, not only the effect from the improved molecular orientation but also the effect resulting from the extension of effective π-conjugation length of the dye (3) should be observed. Therefore, comparison of spectroscopic properties of dyes whose planarity are thought not to be improved and those of dyes whose planarity should be improved by the intercalation were made, both in solution and in films consisting of the dyes and SSA. As representatives of the former group of dyes, 1,3'-diethyl-4,4'-(9,9-diethyl-2,7-fluorenediyl-2,1-ethenediyl)dipyridinium perchlorate (FL, Figure 1-17) and 1,3'-diethyl-2,2'-carbocyanine iodide (pseudoisocyanine; PIC, Figure 1-17) have been selected. The π-electron systems of these dyes are rigid and planar even in solution, and thus the extent of conjugation is expected to be similar both in solution and film states.

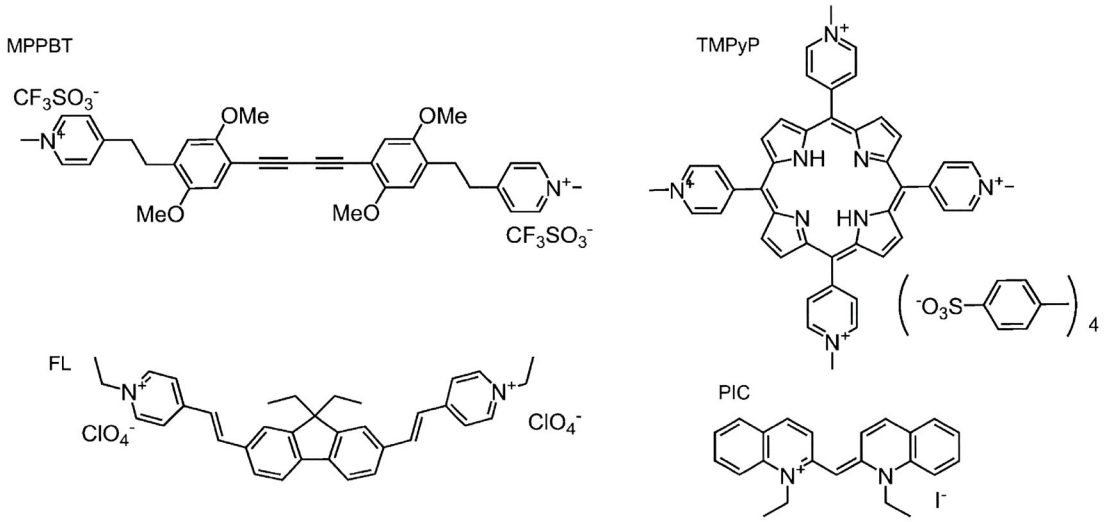


**Figure 1-17** Chemical structure of MPPBT, FL, TMPyP and PIC.

As examples of the latter group of dyes, MPPBT and tetrakis(1-methylpyridinium-4-yl)porphyrin *p*-toluenesulfonate (TMPyP, Figure 1-17) were selected. It is reported for TMPyP that four pyridyl rings and the central porphyrin ring are in the same plane when TMPyP has forms a composite with SSA, whereas the pyridine rings of TMPyP are perpendicular to the plane of porphyrin ring in solution[71]. Therefore, similar to MPPBT, the π-electron system of TMPyP should be also extended in the composite film. One- and two-photon absorption, and XRD measurements were conducted so as to understand the factors that enhance $\sigma^{(2)}_{peak}$ of the dyes in the interlayer space of SSA. The results show that the $\sigma^{(2)}_{peak}$ of all the dyes intercalated in clay films fabricated by the present protocol was found to be enhanced because of factor (2), where the π-plane of the molecules and the direction of electric field of incident light lie in the same plane, and occasionally because of factor (4), te hydrophobic environment of the interlayer space of clay minerals. The $\sigma^{(2)}_{peak}$ of dyes in the present films, enhanced by the two above factors, were from two to three times larger than that in solution. A much more drastic enhancement of $\sigma^{(2)}_{peak}$ was observed from dyes of which planarity were improved by incorporating into the interlayer space of the clay mineral. For such dyes, not only the factors (2) and (4), but also the factors, (3) - extension of the π-conjugated system due to the

improved planarity - and (5), the result of a decrease of the detuning energy, effectively contributed to the enhancements of $\sigma^{(2)}_{peak}$. In particular, the $\sigma^{(2)}_{peak}$ of TMPyP was found to be enhanced up to 13 times in the composite film.

## Reference


(1) Kawasaki, M. & Tanaka, I. Chapter 9 Photochemistry of multi-photon excitation. in *Bunshikagaku Kouza Vol. 11.* (eds Ooshika, U. & Tanaka, I.) 245 (Kyoritsu shuppan, Tokyo, 1987).

(2) Goppert-Mayer, V.M.; *Annalen der Physik*, **1931**, 9, 273.

(3) Kaiser, W., Garrett, C.G.B.; *Phys. Rev. Lett.*, **1961**, 7, 229.

(4) Maruo, S., Nakamura, O., Kawata, S.; *Opt. Lett.*, **1997**, 22, 132.

(5) Walker, E., Rentzepis, P.M.; *Nat. Photonics*, **2008**, 2, 406.

(6) Jia, B., Buso, D., Embden, J.V., Gu, M.; *Adv. Mater.*, **2010**, 22, 2463.

(7) Shiono, T., Itoh, T., Nishino, S.; *Jpn. J. Appl. Phys.*, **2005**, 44, 3559.

(8) Corredor, C.C., Huang, Z.-L., Belfield, K.D., Morales, A.R., Bondar, M.V.; *Chem. Mater.*, **2007**, 19, 5165.

(9) Akiba, M., Dvornikov, A., Rentzepis, P.M.; *Proc. of SPIE*, **2006**, 6331, 63310F.

(10) Shida, N., Higuchi, T., Hosoda, Y., Miyoshi, H., Nakano, A., Tsuchiya, K.; *Jpn. J. Appl. Phys.*, **2004**, 43, 4983.

(11) Terao, M., Morikawa, T., Ohta, T.; *Jpn. J. Appl. Phys.*, **2009**, 48, 080001.

(12) Wang, M.M., Esener, S.C.; *Appl. Opt.*, **2000**, 39, 1826.

(13) Wang, M.M., Esener, S.C.; *Appl. Opt.*, **2000**, 39, 1835.

(14) Coenjarts, C., Ober, C.K.; *Chem. Mater.*, **2004**, 16, 5556.

(15) Galajda, P., Ormos, P.; *Appl. Phys. Lett.*, **2002**, 80, 4653.

(16) Nguyen, L.H., Straub, M., Gu, M.; *Adv. Funct. Mater.*, **2005**, 15, 209.

(17) Kawata, S., Sun, H.-B., Tanaka, T., Takada, K.; *Nature*, **2001**, 412, 697.

(18) Juodkazis, S., Mizeikis, V., Misawa, H.; *J. Appl. Phys.*, **2009**, 106, 051101.

(19) Denk, W., Strickler, J.H., Webb, W.W.; *Science*, **1990**, 248, 73.

(20) Wang, X., Krebs, L.J., Al-Nuri, M., Pudavar, H.E., Ghosal, S., Liebow, C., Nagy, A.A., Schally, A.V., Prasad, P.N.; *Proc. Natl. Acad. Sci. U. S. A.*, **1999**, 96, 11081.

(21) Morales, A.R., Schafer-Hales, K.J., Marcus, A., Belfield, K.D.; *Bioconjug. Chem.*, **2008**, 19, 2559.

(22) Tian, Y.S., Lee, H.Y., Lim, C.S., Park, J., Kim, H.M., Shin, Y.N., Kim, E.S., Jeon, H.J., Park, S.B., Cho, B.R.; *Angew. Chem.*, **2009**, 48, 8027.

(23) Belov, V.N., Bossi, M.L., Folling, J., Boyarskiy, V.P., Hell, S.W.; *Chem. Eur. J.*, **2009**, 15, 10762.

(24) Bhawalkar, J.D., Kumar, N.D., Zhao, C.F., Prasad, P.N.; *J. Clin. Laser Med. Surg.*, **1997**, 15, 201.

(25) Arnbjerg, J., Johnsen, M., Frederiksen, P.K., Braslavsky, S.E., Ogilby, P.R.; *J. Phys. Chem. A*, **2006**, 110, 7375.

(26) Ogawa, K., Hasegawa, H., Inaba, Y., Kobuke, Y., Inouye, H., Kanemitsu, Y., Kohno, E., Hirano, T., Ogura, S.-i., Okura, I.; *J. Med. Chem.*, **2006**, 49, 2276.

(27) Brown, S.B., Brown, E.A., Walker, L.; *Lancet Oncol.*, **2004**, 5, 497.

(28) Walker, A.C., Kar, A.K., Ji, W., Keller, U., Smith, S.D.; *Appl. Phys. Lett.*, **1986**, 48, 683.

(29) Harter, D.J., Band, Y.B.; *Springer Series in Chemical Physics*, **1984**, 38, 102.

(30) Harter, D.J., Shand, M.L., Band, Y.B.; *J. Appl. Phys.*, **1984**, 56, 865.

(31) Lin, T.-C., Chen, Y.-F., Hu, C.-L., Hsu, C.-S.; *J. Mater. Chem.*, **2009**, 19, 7075.

(32) Rumi, M., Ehrlich, J.E., Heikal, A.A., Perry, J.W., Barlow, S., Hu, Z., McCord-Maughon, D., Parker, T.C., Rockel, H., Thayumanavan, S., Marder, S.R., Beljonne, D., Bredas, J.L.; *J. Am. Chem. Soc.*, **2000**, 122, 9500.

(33) Ohta, K., Kamada, K.; *J. Chem. Phys.*, **2006**, 124, 124303.

(34) Turro, N.J. Radiative transitions-the absorption and emission of light. in *Modern Molecular Photochemistry*. (ed Turro, N.J.) 76-152 (University Science Books, California, 1991).

(35) Morales, A.R., Belfield, K.D., Hales, J.M., Van Stryland, E.W., Hagan, D.J.; *Chem. Mater.*, **2006**, 18, 4972.

(36) Ogawa, K., Ohashi, A., Kobuke, Y., Kamada, K., Ohta, K.; *J. Am. Chem. Soc.*, **2003**, 125, 13356.

(37) Drobizhev, M., Stepanenko, Y., Dzenis, Y., Karotki, A., Rebane, A., Taylor, P.N., Anderson, H.L.; *J. Am. Chem. Soc.*, **2004**, 126, 15352.

(38) Karotki, A., Drobizhev, M., Dzenis, Y., Taylor, P.N., Anderson, H.L., Rebane, A.; *Phys. Chem. Chem. Phys.*, **2004**, 6, 7.

(39) Drobizhev, M., Stepaneko, Y., Rebane, A., Wilson, C.J., Screen, T.E., Anderson, H.L.; *J. Am. Chem. Soc.*, **2006**, 128, 12432.

(40) Akiba, M., Morinaga, N., Takizawa, H., Ogiyama, M., Ichijima, S., Tani, T., Harada, A., Inagaki, Y.; *Nonlinear Opt., Quantum Opt.,*, **2005**, 34, 179.

(41) Takizawa, H., Akiba, M., Tani, T., Kawamata, J., Kobayashi, K., Kawahara, K.; *United States Patent*, **2004**, 20040131969.

(42) Boni, L.D., Misoguti, L., Zilio, S.C., Mendonca, C.R.; *Chem. Phys. Chem.*, **2005**, 6, 1121.

(43) Iwase, Y., Kamada, K., Ohta, K., Kondo, K.; *J. Mater. Chem.*, **2003**, 13, 1575.

(44) Audebert, P., Kamada, K., Matsunaga, K., Ohta, K.; *Chem. Phys. Lett.*, **2003**, 367, 62.

(45) Andrade, A.A., Yamaki, S.B., Misoguti, L., Zilio, S.C., Atvars, T.D.Z., Oliveira, O.N., Mendonca, C.R.; *Opt. Mater.*, **2004**, 27, 441.

(46) Kato, S.-i., Matsumoto, T., Shigeiwa, M., Grohmaru, H., Maeda, S., Ishi-i, T., Mataka, S.; *Chem. Eur. J.*, **2006**, 12, 2303.

(47) Badaeva, E.A., Timofeeva, T.V., Masunov, A., Tretiak, S.; *J. Phys. Chem.*, **2005**, 109, 7276.

(48) Kim, O.-K., Lee, K.-S., Woo, H.Y., Kim, K.-S., He, G.S., Swiatkiewicz, J., Prasad, P.N.; *Chem.*

*Mater.*, **2000**, 12, 284.

(49) Reinhardt, B.A., Brott, L.L., Clarson, S.J., Dillard, A.G., Bhatt, J.C., Kannan, R., Yuan, L., He, G.S., Prasad, P.N.; *Chem. Mater.*, **1998**, 10, 1863.

(50) Abbotto, A., Beverina, L., Bradamante, S., Facchetti, A., Pagani, G.A., Bozio, R., Ferrante, C., Pedron, D., Signorini, R.; *Synth. Met.*, **2003**, 139, 795.

(51) Albota, M., Beljonne, D., Brédas, J.L., Ehrlich, J.E., Fu, J.Y., Heikal, A.A., Hess, S.E., Kogej, T., Levin, M.D., Marder, S.R., McCord-Maughon, D., Perry, J.W., Röckel, H., Rumi, M., Subramaniam, G., Webb, W.W., Wu, X.L., Xu, C.; *Science*, **1998**, 281, 1653.

(52) Hayek, A., Nicoud, J.-F., Bolze, F., Bourgogne, C., Baldeck, P.L.; *Angew. Chem.*, **2006**, 118, 6616.

(53) Kishi, R., Nakano, M., Yamada, S., Kamada, K., Ohta, K., Nitta, T., Yamaguchi, K.; *Chem. Phys. Lett.*, **2004**, 393, 437.

(54) Shao, P., Huang, Z., Li, J., Chen, S., Luo, J., Qin, J., Liu, B.; *Opt. Mater.*, **2006**, 29, 337.

(55) Cohanoschi, I., Belfield, K.D., Hernandez, F.; *Chem. Phys. Lett.*, **2005**, 406, 462.

(56) Ahn, T.K., Kim, K.S., Kim, D.Y., Noh, S.B., Aratani, N., Ikeda, C., Osuka, A., Kim, D.; *J. Am. Chem. Soc.*, **2006**, 128, 1700.

(57) Drobizhev, M., Karotki, A., Dzenis, Y., Rebane, A.; *J. Phys. Chem. B*, **2003**, 107, 7540.

(58) Webster, S., Odom, S.A., Padilha, L.A., Przhonska, O.V., Peceli, D., Hu, H., Nootz, G., Kachkovski, A.D., Matichak, J., Barlow, S., Anderson, H.L., Marder, S.R., Hagan, D.J., Stryland, E.W.V.; *J. Phys. Chem. B*, **2009**, 113, 14854.

(59) Raymond, J.E., Bhaskar, A., Goodson III, T., Makiuchi, N., Ogawa, K., Kobuke, Y.; *J. Am. Chem. Soc.*, **2008**, 130, 17212.

(60) Hirakawa, S., Kawamata, J., Suzuki, Y., Tani, S., Murafuji, T., Kasatani, K., Antonov, L., Kamada, K., Ohta, K.; *J. Phys. Chem. A*, **2008**, 112, 5198.

(61) Wada, S.-i. Chemical and Physical Properties of Clay. in *Nendo Handbook 2nd edition*. (ed Nagasawa, K.) 107-150 (Gihodo shuppan, Tokyo, 1994).

(62) Ogawa, M. Smectite and Vermiculite. in *Recent Trend of Functional Clay Materials 1st edition.* (ed Ogawa, M.) 3-15 (CMC Publishing, Tokyo, 2010).

(63) Sasai, R., Itoh, T., Ohmori, W., Itho, H., Kusunoki, M.; *J. Phys. Chem. C*, **2009**, 113, 415.

(64) Sasai, R., Iyi, N., Fujita, T., Arbeloa, F.L., Martinez, V.M., Takagi, K., Itoh, H.; *Langmuir*, **2004**, 20, 4715.

(65) Kiyosawa, K., Shiraishi, N., Shimada, T., Masui, D., Tachibana, H., Takagi, S., Ishitani, O., Tryk, D.A., Inoue, H.; *J. Phys. Chem. C*, **2009**, 113, 11667.

(66) Takagi, S., Eguchi, M., Inoue, H.; *J. Photochem. Photobio. C*, **2006**, 7, 104.

(67) Kamada, K., Tanamura, Y., Ueno, K., Ohta, K., Misawa, H.; *J. Phys. Chem. C*, **2007**, 111, 11193.

(68) Suzuki, Y., Hirakawa, S., Sakamoto, Y., Kawamata, J., Kamada, K., Ohta, K.; *Clays Clay Miner.*, **2008**, 56, 487.

(69) Suzuki, Y., Nakagawa, K., Nishioka, Y., Tenma, Y., Kawamata, J.; *Clay Science*, **2010**, 14, 229.

(70) Tarutani, H., Tanaka, Y., Kawamata, J.; *PACIFICHEM 2010*, **2010**, 1942.

(71) Takagi, S., Shimada, T., Eguchi, M., Yui, T., Yoshida, H., Tryk, D.A., Inoue, H.; *Langmuir*, **2002**, 18, 2265.

# Chapter 2 Fabrication of Low Light-Scattering Inorganic/Organic Composites Suitable for Nonlinear Optical Measurements

## 2-1 Introduction

Among inorganic-layered-compound/organic composites, the clay/dye composite films fabricated by Takagi et al. are known to possess relatively low light-scattering properties[1,2] and layer-by-layer stacking. Such films can be fabricated through a simple protocol as described below. First, the clay/dye composites are prepared by mixing an aqueous dispersion of an exfoliated clay mineral with a solution of an organic compound. By using an exfoliated clay mineral, homogeneous adsorption of dyes onto the clay layers can be obtained. This homogeneity results in layer-by-layer stacking of composites in the following film fabrication process. The clay/dye composite films can be prepared by filtration of the aqueous dispersion of the clay/dye composites. Although a film obtained by this protocol was transparent, it was unsuitable for NLO device applications, because the incoherent light-scattering typically observed in transparent but light-scattering media such as colloids needs to be suppressed. Furthermore, the laser beam must be propagated in the media without changing its mode and profile.

In this study, fabrication of highly low light-scattering inorganic/organic hybrid materials has been attempted. Previously, a novel method, based on the Langmuir-Blodgett technique, for fabricating a film consisting of organic nano-crystals satisfactory for NLO devices has been reported[3-5]. In the films obtained by this technique, organic nano-crystals were densely accumulated. When the sizes of the organic nano-crystal itself and the gap between the organic nano-crystals were sufficiently small compared to the wavelength of light, incoherent light-scattering was considerably suppressed. This fact suggests that a film consisting of clay/dye composites which satisfies the following requirements should possess extremely low light-scattering properties: (i) the size of the particles

which constitute the film should be appropriately smaller than the wavelength of light and (ii) the size of gaps between the particles is also smaller than the wavelength of light. In this study, the fabrication conditions of the composite film have been optimized in order to satisfy the above two requirements.

It is reported that exfoliated clay mineral particles tend to aggregate when they adsorb organic molecules in a dispersion[6]. Furthermore, addition of organic solvent into a water dispersion of exfoliated clay mineral also promotes the aggregation of clay mineral particles[6]. Therefore, control of the size of the aggregate is the most important issue to be optimized for obtaining low light-scattering films. The appropriate size of the aggregates is expected to be a larger size than the pore size of the membrane filter and a smaller size than the wavelength of light. The pore size of a commonly available membrane filter is 100 nm. Therefore, the appropriate size of the aggregates was targeted to be ~150 nm. Factors which determine the size of the aggregates are the size of the clay particle, concentration of the clay in the dispersion and the amount of organic compounds adsorbed onto clay particles. Furthermore, if the organic compounds were added not as water solution but as organic solvent solution, the amount of the added solvent is also an important factor. Thus, the factors were optimized so as to obtain aggregates with the average size of 150 nm. The resulting films obtained by this strategy were found to possess very low light-scattering properties suitable for NLO devices.

## 2-2 Fabrication

### 2-2-1 Composites

The clay/dye composites were prepared by mixing an aqueous dispersion of a clay mineral with a solution of an organic dye. The details of the preparation conditions such as concentrations of dispersion and solution, type of solvent and so forth will be discussed latter.

### 2-2-2 Films

The clay/dye composite films were fabricated by filtration of the aqueous dispersion of clay/dye composites under suction with a mixed cellulose ester membrane filter (ADVANTEC, A010A025A; 100 nm pore size, 25 mm diameter). This is a commonly available membrane filter with the smallest pore size. The film deposited on the membrane filter was peeled off from the filter as a self-standing film. The film was placed onto a fused silica substrate for optical measurements.

### 2-2-3 Materials

#### 2-2-3-1 Clay Minerals

The size of the exfoliated clay mineral particle should play a significant role in the light-scattering properties of the obtained film. Therefore, the properties of films fabricated by employing clay minerals with a smaller or a larger particle size than the wavelength of light were compared.

As a clay mineral with a small particle size, SSA (Kunimine Ind. Co. Ltd., Japan) was used without further purification. The stoichiometric formula for SSA is $[(Si_{7.20}Al_{0.80})(Mg_{5.97}Al_{0.03})O_{20}(OH)_4]^{0.77-}\cdot(Na_{0.49}Mg_{0.14})^{0.77+}$, the surface area was 750 $m^2g^{-1}$, and the CEC was 0.997 meq $g^{-1}$. An atomic force microscope (AFM) image of a casted film obtained from the dispersion of SSA in ultra pure water at a concentration of 0.11 g $l^{-1}$ is shown in Figure 2-1. Most of clay mineral particles were found to form a cluster with a typical diameter of 1 μm through evaporation of water. However, the

height of the cluster of SSA, ca. 1.4 nm, corresponded to the thickness of hydrated exfoliated single clay mineral layer. This fact suggests that the SSA was exfoliated into single layers in the dispersion at this concentration. Thus, in this study, an aqueous dispersion of clay mineral with the concentration lower than 0.11 g $l^{-1}$ was used. Also, small white dots around the clusters can be seen in Figure 2-1. It is natural to suppose that these are clay mineral particles which did not form the cluster. The average diameter in the in-plane direction of the dots was ~30 nm. This size corresponded to that of SSA provided by the manufacturer.

As for a clay mineral with a large particle size, natural sodium montmorillonite (Kunipia-P, Kunimine Ind. Co. (Japan), CEC: 1.17 meq $g^{-1}$) was employed. The stoichiometric formula for the Kunipia-P is $[(Na_{0.49}Mg_{0.14})[(Si_{7.70}Al_{0.30})(Al_{3.12}Mg_{0.68}Fe_{0.19})O_{20}(OH)_4]$. Similar to the case of SSA, Kunipia-P was exfoliated into single layers at a concentration of 0.11 g $l^{-1}$. The average diameter of the exfoliated Kunipia-P particles measured by AFM was ~1 μm.

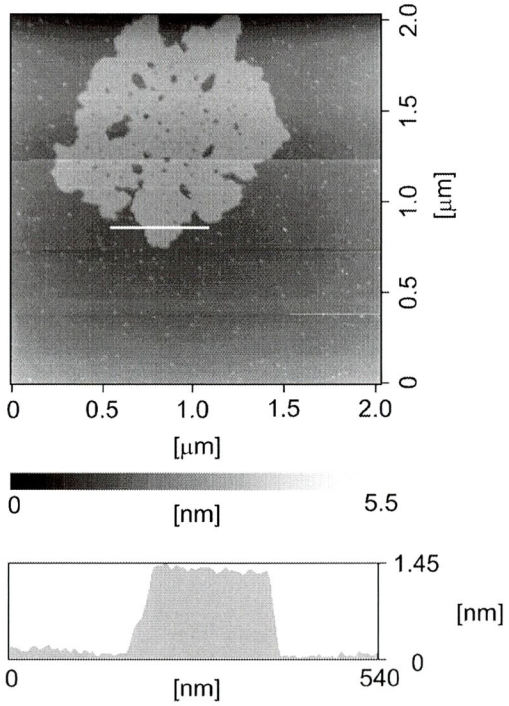


**Figure 2-1** Atomic force microscopy image of a cast film obtained from the dispersion of SSA (before adsorbing an organic compound) at a concentration of 0.11 g $l^{-1}$ (top). Cross-sectional image of a selected region (white line in the top image) is also shown (bottom).

### 2-2-3-2 Organic compounds

**Tris(1,10-phenanthroline)ruthenium(II) dichloride ($[Ru(phen)_3]Cl_2$; Figure 2-2(a))**

The synthesis and resolution of the cationic ruthenium(II) complex, $[Ru(phen)_3]Cl_2$, was performed according to the reported method[7,8]. The compound was identified by uv-visible and circular dichroism spectra and $^1H$ NMR. The optical purity of the compound was estimated to be higher than 98 % for both enantiomers. Clay/$Ru(phen)_3$ composites were prepared by mixing water dispersion of a clay mineral with a water solution of $Ru(phen)_3$.

**1,4-Bis(2,5-dimethoxy-4-{2-[4-(*N*-methyl)pyridinium]ethenyl}phenyl)butadiyne triflate (MPPBT; Figure 2-2(b))[9]**

MPPBT supplied from Dr. K. Kamada (National Institute of Advanced Industrial Science and Technology, Osaka, Japan) was used without further purification. Since the solubility of MPPBT in water is low, it had to be dissolved in a water miscible organic solvent. However, addition of a large amount of organic solvent into a water dispersion of clay minerals prevents exfoliation of clay minerals into single sheets. Therefore, MPPBT was dissolved in dimethylsulfoxide (DMSO), a solvent that can dissolve MPPBT with a high concentration. The highest concentration of the solution used in this study was $2 \times 10^{-3}$ mol $l^{-1}$. The clay/MPPBT composites were prepared by mixing an aqueous dispersion of a clay mineral with small amount of a highly concentrated DMSO solution of MPPBT.

**1,1'-Diethyl-4,4'-(9,9-diethyl-2,7-fluorenediyl-2,1-ethenediyl)dipyridinium perchlorate (FL; Figure 2-2 (c))**

FL was synthesized according to procedures previously reported in the literature[10]. Since the solubility of FL in water is low, FL was also dissolved in DMSO at a maximum concentration of 1 mmol $l^{-1}$.

**Tetrakis(1-methylpyridinium-4-yl)porphyrin *p*-toluenesulfonate (TMPyP, Figure 2-2 (d))**

TMPyP was purchased from Aldrich and was used without further purification. The solubility of TMPyP in water was sufficient for fabricating composites. Hence water was used as the solvent for TMPyP.

**1,1'-Diethyl-2,2'-cyanine iodide (Pseudoisocyanine (PIC); Figure 2-2 (e))**

PIC was purchased from Kanto Kagaku and was used without further purification. A water solution of PIC was mixed with aqueous dispersion of a clay mineral.

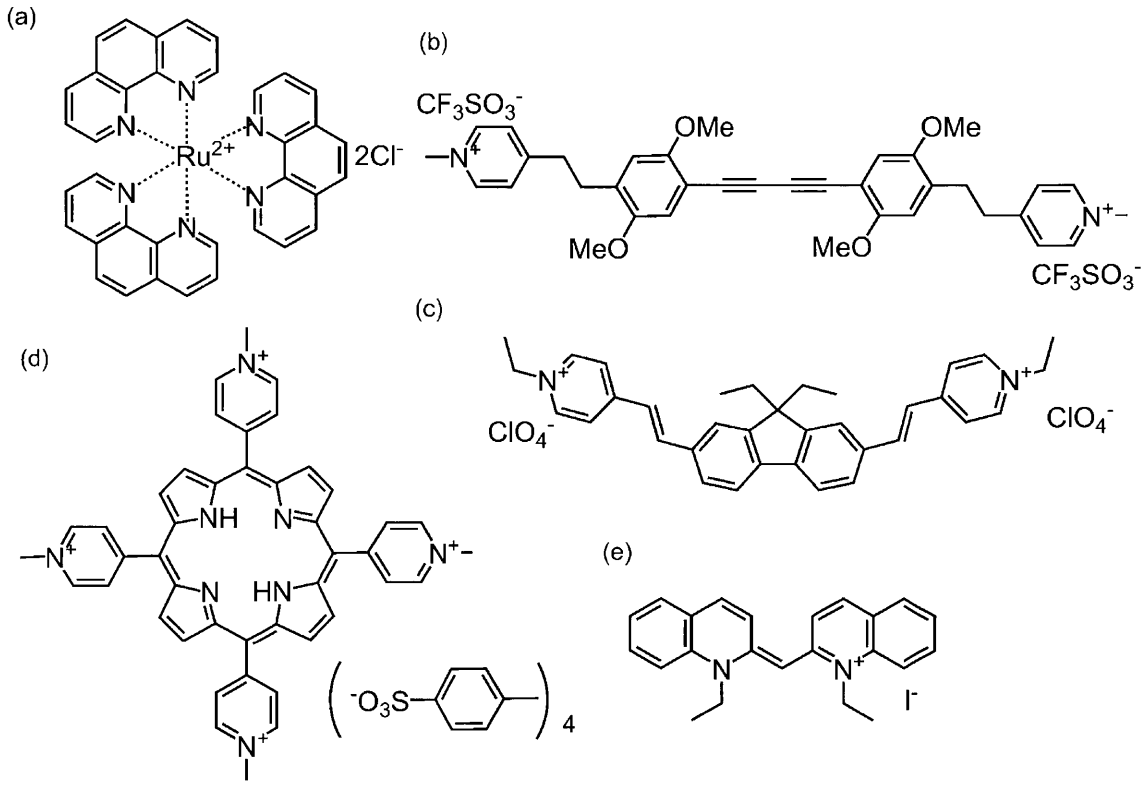


**Figure 2-2** Chemical structure of $[Ru(phen)_3]Cl_2$(a), MPPBT(b), FL(c), TMPyP(d) and PIC(e).

## 2-3 Light-Scattering Properties of the Prepared Films

### — Optimization of Film Fabrication Conditions for Obtaining the Low Light-Scattering Films —

As described earlier, the size of the aggregates should be optimized in order to obtain a low light-scattering film. The appropriate size of the aggregates is expected to be a larger size than the pore size of the membrane filter and a smaller size than the wavelength of light. Due to the low water solubility of MPPBT and FL, clay/MPPBT and clay/FL composites were fabricated by adding a DMSO solution of MPPBT or FL to a water dispersion of a clay mineral, as described previously. Depending on the volume percentage of DMSO in the resulting dispersion, the size of the aggregates should vary. Therefore, the differences in the size of the aggregates produced, employing MPPBT as an organic compound, as a function of the volume percentage of DMSO in the composite dispersion were examined by AFM measurements., For example, composites obtained from DMSO (10% v/v)-water mixed solvent were prepared by mixing 18 ml of an aqueous dispersion of a clay mineral (0.11 g $l^{-1}$) with 2 ml of a DMSO solution of MPPBT ($10^{-4}$ mol $l^{-1}$). Those from a DMSO (1% v/v)-water mixed solvent were prepared by mixing 19.8 ml of aqueous dispersion of a clay mineral (0.10 g $l^{-1}$) with 0.2 ml of a DMSO solution of MPPBT ($10^{-3}$ mol $l^{-1}$), and so forth . In order to avoid excess aggregation, the measurements were made immediately after adding a DMSO solution of MPPBT to a water dispersion of a clay mineral. The %CEC of MPPBT was fixed to be 20% in this investigation. Therefore all MPPBT molecules were assumed to be adsorbed onto the SSA. As shown in Figure 2-3, the average sizes of the aggregates were found to be 1 μm, 200 nm, 150 nm and 100 nm when the volume percentages of DMSO in DMSO-water mixed solvent were 10, 5, 1 and 0.5% v/v, respectively. The deviation of the size of aggregates was within 30%. Since the pore size of the membrane filter employed was 100 nm, the aggregates obtained at the volume percentages of DMSO in the mixed solvent of 0.5% v/v were not adequate, as some aggregates were smaller than

the pore size of the membrane filter and would pass through it. In fact, when the volume percentages of DMSO in the resulting dispersion were less than 1% v/v, the filtrates were orange which could be attributed to the presence of MPPBT in the filtrate. On the other hand, when the volume percentages of DMSO in the resulting dispersion were higher than 1% v/v, the filtrates were colourless. This indicates the obtained composites were completely trapped on the membrane filter. From the viewpoint of light scattering, the size of the aggregate should be minimized. Thus, the film consisting of composites obtained from DMSO (1% v/v)-water mixed solvent was found to be appropriate when a membrane filter whose pore size is 100 nm was employed.

Figure 2-4 shows absorption spectra of a DMSO solution of MPPBT and composite films of SSA/MPPBT obtained from 10 and 1 % v/v DMSO-water mixed solvents. Compared to the spectrum of MPPBT in DMSO, those in the composite films were found to red shift, as reported previously[11,12].

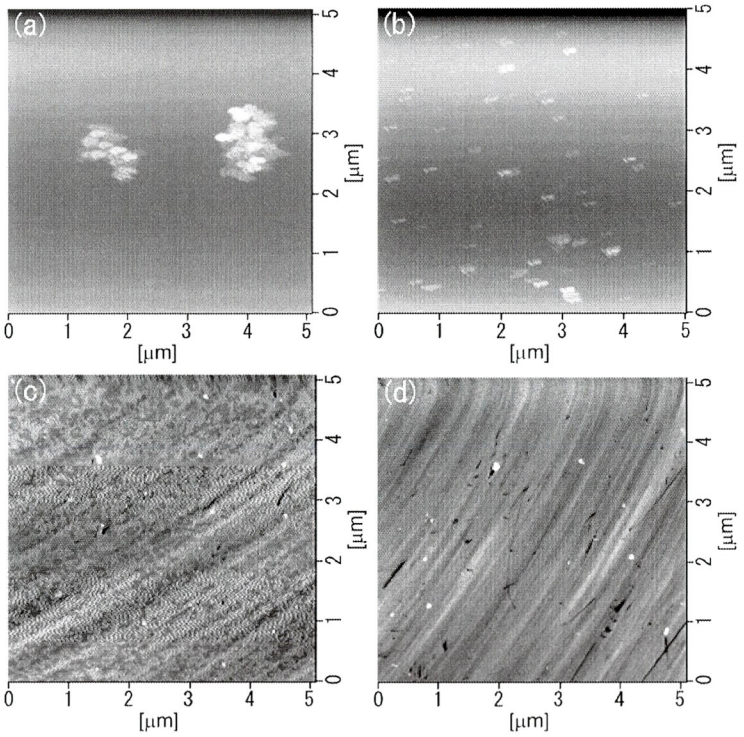


**Figure 2-3** AFM images of SSA–MPPBT composites fabricated in (a) 10, (b) 5, (c) 1 and (d) 0.5% v/v DMSO–water mixed solvent. Composites were spin-coated on mica ((a) and (b)) or fused-silica ((c) and (d)) substrates.

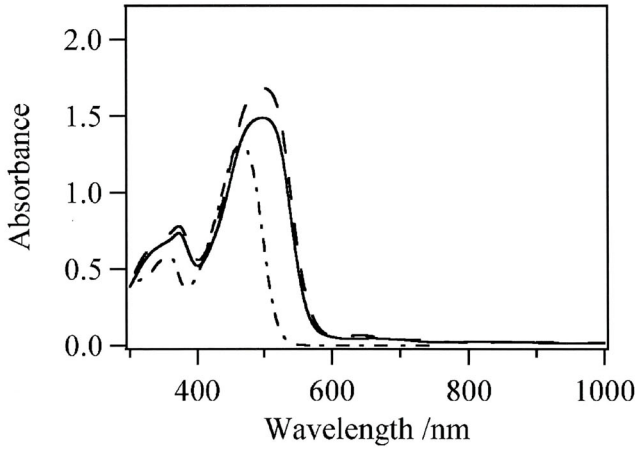


**Figure 2-4** Absorption spectra of MPPBT in DMSO and in films. DMSO solution (dot-dashed lines); MPPBT–SSA hybrid film from DMSO (1% v/v)–water mixed solvent (dashed line), MPPBT–SSA hybrid film from DMSO (10% v/v)–water mixed solvent (solid line).

Spectra observed for both composite films seemed to be almost the same. In both cases, the absorbance of the films in the wavelength region longer than 700 nm, where MPPBT absorbs no light, was nearly zero, indicating that the films were almost transparent.

However, NLO measurements revealed some differences between the various films. Figure 2-5(a) shows open-aperture Z-scan patterns (see Appendix) of the films observed using a laser beam at a wavelength of 760 nm. From the film obtained from 1 % v/v DMSO-water mixed solvent, a regularly shaped trace as theoretically expected for the measurement was observed. Namely, transmittance was reduced only when the sample was located near the focal point. The SSA/MPPBT composite film obtained in this condition was found to exhibit excellent light scattering properties suitable even for NLO materials. On the one hand, a trace similar to that observed for a closed-aperture Z-scan pattern was typically observed for the film obtained from 10 % v/v DMSO-water mixed solvent, even though the measurement was an open-aperture Z-scan (Figure 2-5(b)). This fact suggests the existence of an inhomogeneity of the refractive index in the film, causing the sample itself to exhibit a lens effect. The most probable reason for the existence of the inhomogeneity is the presence of a gap between the particles in the film due to the large size of

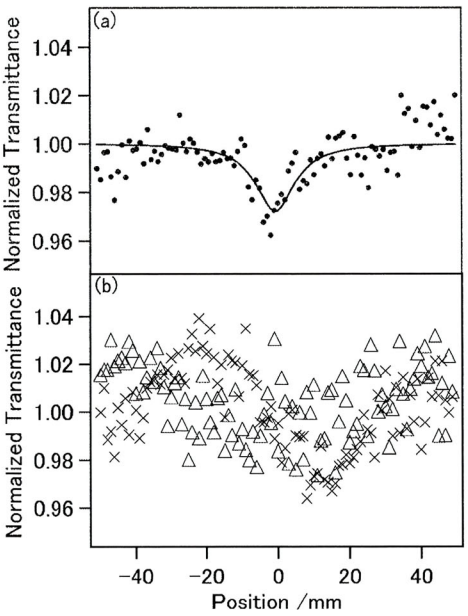


**Figure 2-5** Open-aperture Z-scan trace for (a) SSA/MPPBT composite film obtained from DMSO (1% v/v)–water mixed solvent (closed circles) and theoretical fit to this trace (solid line), and (b) SSA/MPPBT composite film obtained from DMSO (10% v/v)–water mixed solvent (crosses) and Kunipia-P/MPPBT composite film from DMSO (1% v/v)–water mixed solvent (open triangles). Patterns shown in (b) do not fit the theoretical curve.

aggregates formed in the 10 % v/v DMSO-water mixed solvent. Occasionally, a regularly shaped trace as theoretically expected for the measurement was observed even for the film obtained from 10 % v/v DMSO-water mixed solvent. This fact indicates that there are some scattering free light paths are possible for a tightly focused laser beam. Therefore, it is not always possible to unambiguously evaluate the TPA characteristics of the film obtained from 10 % v/v DMSO-water mixed solvent. However, such a light path can rarely be found. Therefore, it is not practical to apply such a film in nonlinear optical measurements.

As can be seen in Figure 2-6, light scattering from a film fabricated employing a clay mineral possessing a large particle size, Kunipia-P, was considerable, though the film was fabricated from a dispersion whose volume percentage of DMSO was only 1%. The observed absorbances seen in a UV-vis measurement of the films were not zero even at a wavelength region where MPPBT absorbed no light (typically, longer than 700 nm). The shorter was the wavelength, the larger the

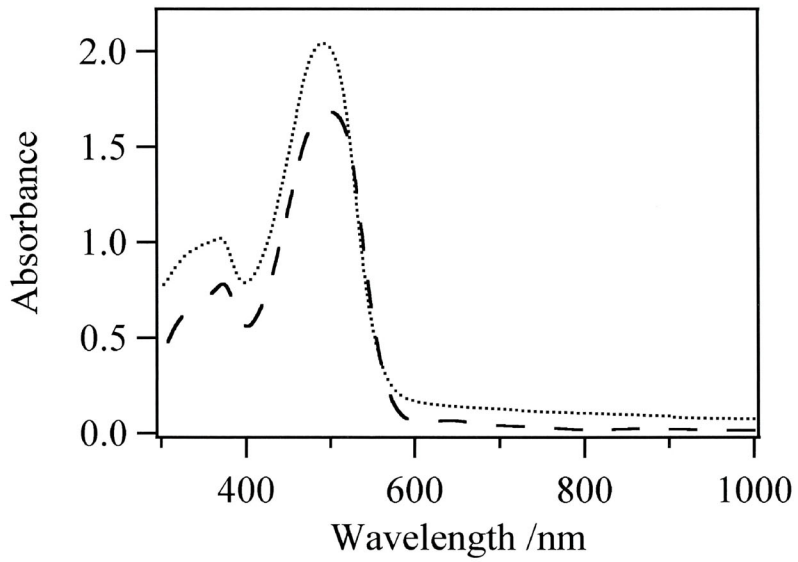


**Figure 2-6** Absorption spectra of MPPBT in films. MPPBT–SSA hybrid film from DMSO (1% v/v)–water mixed solvent (dashed line), and the MPPBT–Kunipia-P hybrid film from DMSO (1% v/v)–water mixed solvent (dotted line).

detected absorbance. This is typical behavior observed for a light scattering sample. Taking into account the considerable amount of light scattering, the trace of the Z-scan pattern seen in Figure 2-5 (b) can not be explained. Furthermore, a regularly shaped trace as theoretically expected for the measurement has never been observed for this type of sample, even though we made considerable numbers of repeat measurements while changing the position of the irradiation spot. As already described, clay minerals adsorbing organic compound tend to aggregate. Therefore, in this case, the size of aggregates should be considerably larger than the wavelength of light. This observation indicates that the use of a clay mineral with a size larger than a wavelength of light is a disadvantageous strategy when fabricating a film by the present protocol.

Consequently, it is concluded that the optimization of the size of the aggregates which are formed when organic compounds are adsorbed onto clay particles is the most important issue to obtain low light-scattering films. The appropriate size of the aggregates was found to be ~150 nm when a membrane filter with the pore size of 100 nm was employed. The resulting films obtained by this strategy were found to possess very low light-scattering properties suitable for NLO devices. The

size of the aggregates was found to depend on the size of the clay particle, the % CEC, the charge density of the clay surface and the hydrophobicity of the surface of the composite. Therefore, in order to fabricate films possessing very low light-scattering properties suitable for NLO devices, optimization of the factors should be made for each organic compound used and for each % CEC. In other words, it is concluded that very low light-scattering films can be fabricated by employing any dyes and inorganic layered compounds at any % CEC if the factors mentioned above have been optimized.

Optimized parameters for preparing aggregates of composites with the size of ~150 nm are summarized in Table 2-1 for all the organic compounds used in this study.

**Table 2-1** Optimized parameters for preparing ~150 nm size of $Ru(phen)_3$-SSA aggregates

| Dyes/Solvents | % CEC (%) | Concentration of dye solution (mM) | Amount of solution mixed with SSA dispersion (ml) | Concentration of SSA dispersion (g / l) | Amount of SSA dispersion mixed with solution (ml) |
|---|---|---|---|---|---|
| $Ru(phen)_3$/Water | 60 | 0.10 | 6.0 | 0.017 | 120 |
| MPPBT/DMSO | 10 | 1.0 | 0.10 | 0.10 | 20 |
| | 20 | 1.0 | 0.20 | 0.050 | 40 |
| | 40 | 1.0 | 0.40 | 0.025 | 80 |
| | 60 | 1.0 | 0.60 | 0.017 | 120 |
| | 80 | 1.0 | 0.80 | 0.013 | 160 |
| FL/DMSO | 10 | 1.0 | 0.10 | 0.10 | 20 |
| | 20 | 1.0 | 0.20 | 0.050 | 40 |
| | 40 | 1.0 | 0.40 | 0.025 | 80 |
| | 60 | 1.0 | 0.60 | 0.017 | 120 |
| | 80 | 1.0 | 0.80 | 0.013 | 160 |
| TMPyP/Water | 10 | 0.050 | 1.0 | 0.10 | 20 |
| | 20 | 0.050 | 2.0 | 0.050 | 40 |
| | 40 | 0.050 | 4.0 | 0.025 | 80 |
| | 60 | 0.050 | 6.0 | 0.017 | 120 |
| | 80 | 0.050 | 8.0 | 0.013 | 160 |
| PIC/Water | 10 | 0.20 | 1.0 | 0.050 | 40 |
| | 20 | 0.20 | 2.0 | 0.025 | 80 |
| | 40 | 0.20 | 4.0 | 0.013 | 160 |
| | 60 | 0.20 | 6.0 | 0.0084 | 240 |
| | 80 | 0.20 | 8.0 | 0.0063 | 360 |

# 2-4 Characteristics of the Low Light-Scattering Films

## 2-4-1 Control of the Thickness of the Film

### 2-4-1-1 SSA/MPPBT Composites

The absorbances of the wavelength of the absorption maxima ($\lambda_{max}$) were plotted against the amount of the filtered dispersion in the inset of Figure 2-7. Not only the $\lambda_{max}$ but also the absorbance over the whole measured range steadily increased as the amount of the filtered dispersion increased. This linear relationship over the whole measured range indicates that the thickness of the film, namely the optical density of the film, can easily be controlled, while keeping its excellent low light-scattering nature and that the film can be fabricated with a high reproducibility. Spin-coated films of organic materials are widely used as optical materials because of their low light-scattering nature. However, fabrication of a thick spin coat film is not easy. This limits the applicability of spin-coated films for devices which require low light-scattering materials with high optical densities. The availability of thick low light-scattering films is a promising advantage of the present film compared to the spin coat films.

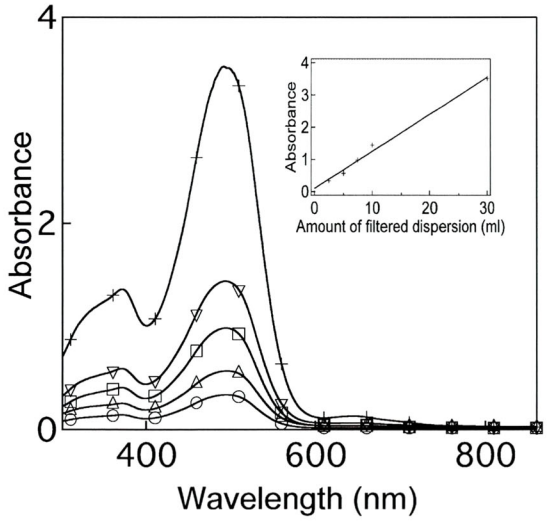


**Figure 2-7** Absorption spectra of SSA/MPPBT composite films (CEC% =20%) fabricated by filtering different amounts of dispersion (2.5 ml (o), 5 ml (Δ), 7.5 ml (□), 10 ml (∇), 30 ml (+)). Absorbance at the $\lambda_{max}$ (498 nm) against the amount of the filtered dispersion are plotted in inset.

### 2-4-1-2 SSA/Ru(phen)$_3$ Composites

The controllability of the film thickness has also been surveyed for the film incorporating of Ru(phen)$_3$. The transparency of the films was ascertained by measuring the absorption spectra as shown in Figure 2-8. The absorbance of the films at the wavelength region longer than 660 nm was nearly zero, where Ru(phen)$_3$ absorbed no light. The inset of Figure 2-8 shows that the absorbance at 450 nm due to the intercalated metal complex increased linearly with the amount filtered, similar to the case of SSA/MPPBT composite films. These observations suggested that the thickness of the film increased uniformly with increase of the filtered amount.

The thickness of the film was estimated from a fringe pattern found in the transmittance spectrum at a near infra-red wavelength region by means of the swanepoel method[13]. The film thicknesses obtained in this way are plotted in the inset of Figure 2-9 against the filtered amount. The transmittance spectra are also shown in Figure 2-9. As expected from the absorption spectra shown in Figure 2-8, the film thickness indeed increased linearly with increasing amount filtered.

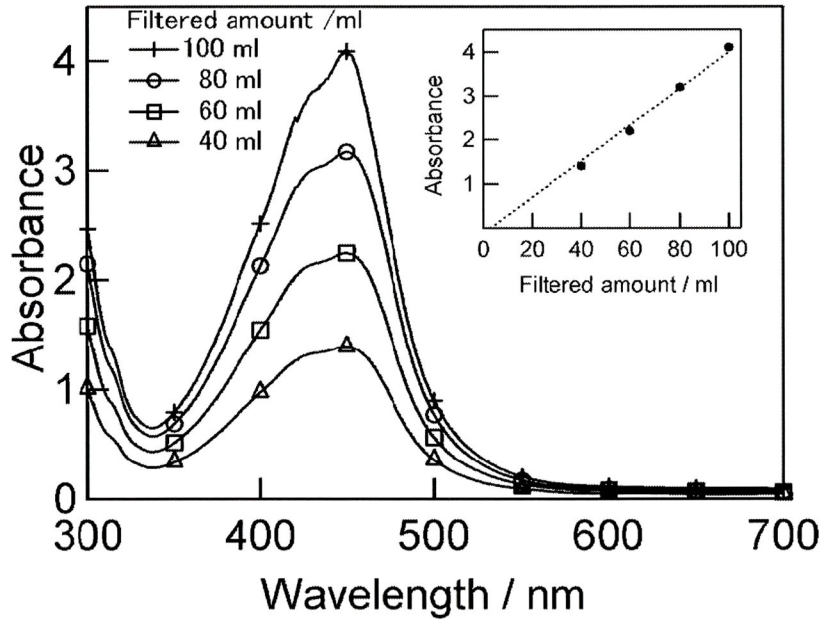


**Figure 2-8** Absorption spectra of SSA/Ru(phen)$_3$ composite films fabricated by filtering various amounts of dispersion (40 ml, 60 ml, 80 ml, 100 ml). The inset is the plot of absorbance at $\lambda_{max}$ (450 nm) vs. the filtered amount.

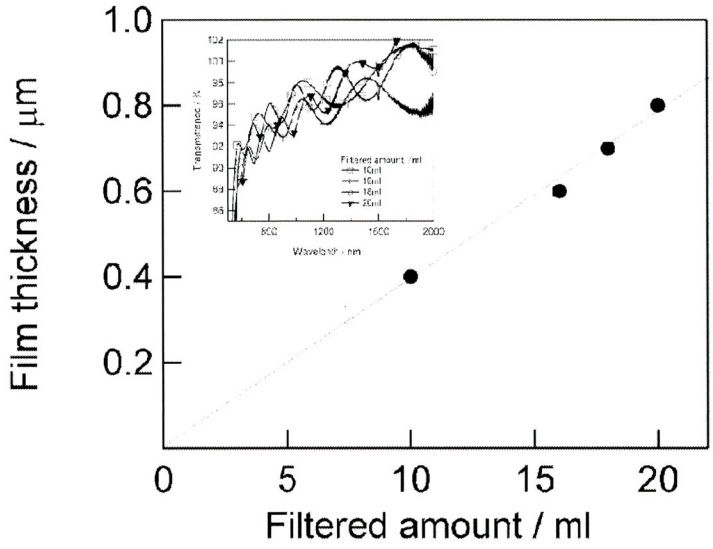


**Figure 2-9** Plot of the thickness of SSA/Ru(phen)$_3$ composite film vs. the filtered amount. Transmittance spectra are shown in the inset.

## 2-4-2 Stacking of Clay Layers in the Film

In this section, let us discuss how the composites stack in the film. Figure 2-10 shows a transmission electron microscopy (TEM) image of the SSA/Ru(phen)$_3$ composite film. The definite layer-by-layer character was confirmed with an interlayer spacing of c.a. 1.8 nm. The layer-by-layer stacking of clay layer was observed to extend over a few micrometers. No information was obtained, however, as to the arrangement of the intercalated metal complexes between the clay layers.

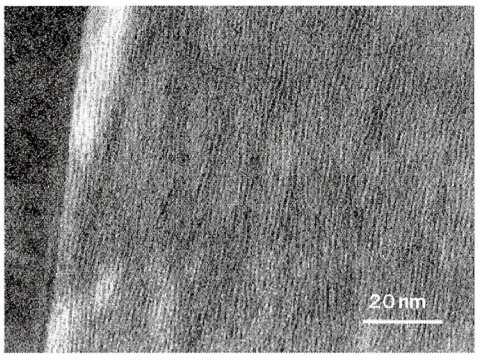


**Figure 2-10** A cross-sectional transmission electron microscopy (TEM) image of the composite film. The cross-sectional thin specimen was prepared using a focused ion-beam (FIB) system (Hitachi FB-2100). The TEM observation was performed using a JEOL JEM-2010 UHR.

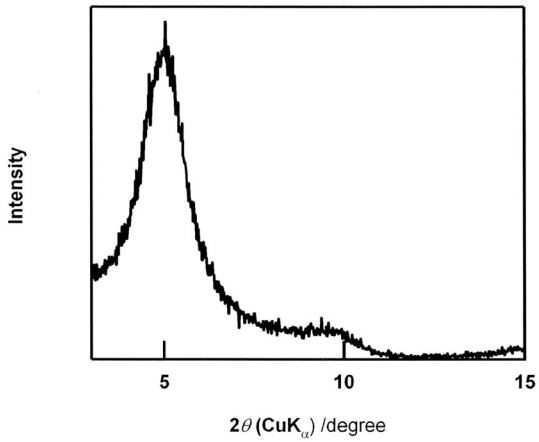


**Figure 2-11** X-ray diffraction patterns for the thin clay film. The peak at $2\theta$(CuK$\alpha$) = 5.1 degree was assigned to (001) diffraction.

Figure 2-11 shows the X-ray diffraction pattern of the composite film, indicating the (001) diffraction at 1.7 nm, which was in accord with the TEM observation. The obtained composite films had a uniform thickness, regular stacking and molecules intercalated in a unique orientation.

## 2-5 Nonlinear Optical (NLO) Properties

### 2-5-1 SSA/Ru(phen)$_3$ Film

Films consisting of a chiral Ru-complex should exhibit optical second-harmonic generation (SHG) activity when the guest molecules arrange in an oriented molecular array. In order to confirm molecular orientation in the present films, SHG measurements were conducted for SSA/Ru(phen)$_3$ composite films[14].

Figure 2-12(a) shows the SHG signals when a repetitively Q-switched pulsed beam from a Nd: YAG laser (Lee 818 TQ) operated at a wavelength of 1064 nm was irradiated onto a film. Notably, a film with intercalating chiral metal complexes gave a signal of significant intensity, while a film with intercalating racemic metal complexes gave a negligible level of signal. This fact indicates that an oriented molecular array of the chiral Ru complex existed in thispresent film. It should be also emphasized that the SHG signal was observed only in a *p-s* optical geometry, in which the p-polarized fundamental beam was irradiated and the *s*-polarized second-harmonic signal was detected. The second-harmonic signals were negligible in *p-p*, *s-p* and *s-s* geometry. This fact indicated that the nonvanishing susceptibility component was solely $\chi^{(2)}_{xyz}$. The second-order nonlinear susceptibility ($\chi^{(2)}_{xyz}$) estimated in a similar way as reported in references 15 and 16 was 0.6 pm $V^{-1}$.

Figure 2-12(b) shows the dependence of the SHG intensity on the film thickness. When the film thickness was smaller than 1 μm, the signal increased in a quadratic way with respect to the film thickness, while it leveled off at the region thicker than 4 μm. The behavior of the present film was interpreted in terms of a SHG-active three-dimensional crystal with the coherence length[17] of c.a. 4 μm. Considering that the typical coherence length of quartz and organic crystals is 20 or 1 μm, respectively[18,19], the estimated value of 4 μm as a coherence length seemed to be reasonable since the present film was a hybrid material consisting of aluminosilicates and organic compounds. The

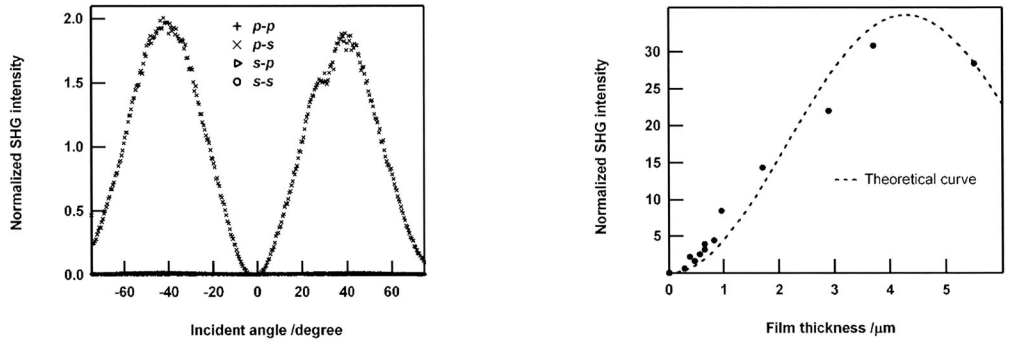


**Figure 2-12** (a) Dependences of the SHG intensity on the incident angle of the laser beam for a film thickness of 0.4 μm recorded in various optical geometries. The vertical axis is normalized by the SHG intensity of the Maker-Fringe pattern of $d_{11}$ of quartz (wedged sample) recorded at the same experimental conditions. (b) Second-harmonic intensity versus the thickness of the film. The filled circles are the experimental data points and the dashed line a $\sin^2$(thickness) fit to the experimental data.

fact that the coherence length dependence of the sample could be estimated means the film can be, as an NLO material, defined not as a thin material but as a bulk material. In other words, the present composite films can be applied to various NLO devices as an organic compound based bulk material.

## 2-5-2 Films Consisting of SSA and Other Dyes

Finally, let us discuss the NLO properties of composites films consisting of other organic compounds than MPPBT and $Ru(phen)_3$. Since those composite films are SHG inactive, Z-scan measurements were conducted. The patterns of SSA/FL, SSA/TMPyP and SSA/PIC composite films are shown in Figure 2-13. Similar patterns as observed from the composite films consisting of MPPBT were observed from all films. This fact indicates that not only films of MPPBT but also of the other organic compounds were sufficiently low light-scattering to be suitable for NLO measurements. Thus, it is concluded that the present film fabrication protocol can generally be utilized to employ various organic compounds for fabricating low light-scattering composites suitable for NLO applications.

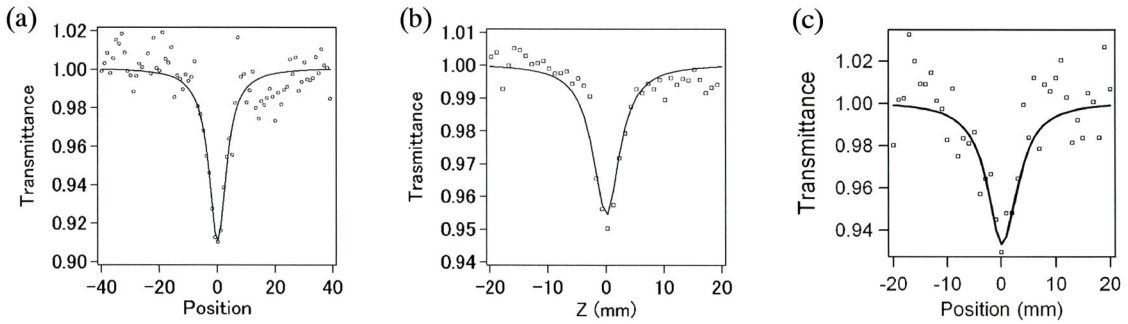


**Figure 2-13** Z-scan patterns of SSA/FL (a), SSA/TMPyP(b) and SSA/PIC(c) composite films. The vertical axis is the transmittance and the horizontal axis is the distance from the focal point, respectively.

## 2-6 Conclusion

In this chapter, a protocol for fabricating a very low light-scattering clay/dye composite film suitable even for NLO materials has been demonstrated. In order to obtain such films, fabrication should be made under highly optimized conditions. Key points to be optimized to obtain such a film are the particle size of the exfoliated clay mineral and the size of the aggregates. When the size of the aggregates was controlled to be about 150 nm, a very low light-scattering film could be fabricated. In principle, this protocol can be applied even when other layered-inorganic compounds are employed as the host. Thus, films fabricated by the present strategy should open a door to apply inorganic-layered-compound/dye composites for optical devices which utilize their promising characteristics.

## References


(1) Takagi, S., Shimada, T., Eguchi, M., Yui, T., Yoshida, H., Tryk, D.A., Inoue, H.; *Langmuir*, **2002**, 18, 2265.

(2) Takagi, S., Eguchi, M., Tryk, D.A., Inoue, H.; *J. Photochem. Photobio. C*, **2006**, 7, 104.

(3) Hirakawa, S., Inada, Y., Tani, S., Ogata, Y., Kawamata, J.; *Nonlinear Opt., Quantum Opt.,*, **2005**, 34, 195.

(4) Hirakawa, S., Hasegawa, S., Inada, Y., Tanaka, Y., Kawamata, J.; *Jpn. J. Appl. Phys.*, **2007**, 46, L1203.

(5) Hasegawa, S., Hirakawa, S., Inada, Y., Kawamata, J.; *J. Nanosci. Nanotechnol.*, **2009**, 9, 216.

(6) Bujdak, J., Janek, M., Madejova, J., Komadel, P.; *Clays Clay Miner.*, **2001**, 49, 244.

(7) Kawamata, J., Yamaki, H., Ohshige, R., Seike, R., Tani, S., Ogata, Y., Yamagishi, A.; *Colloids Surf. A*, **2008**, 321, 65.

(8) Mason, F.S. (ed) *Molecular Chiral Activity and the Chiral Discriminations*. (Cambridge University Press, Cambridge, 1982).

(9) Iwase, Y., Kamada, K., Ohta, K., Kondo, K.; *J. Mater. Chem.*, **2003**, 13, 1575.

(10) Kamada, K., Tanamura, Y., Ueno, K., Ohta, K., Misawa, H.; *J. Phys. Chem. C*, **2007**, 111, 11193.

(11) Suzuki, Y., Hirakawa, S., Sakamoto, Y., Kawamata, J., Kamada, K., Ohta, K.; *Clay. Clay Miner.*, **2008**, 56, 487.

(12) Swanepoel, R.J.; *J. Phys. E: Sci. Instrum.*, **1983**, 16, 1214.

(13) Suzuki, Y., Matsunaga, R., Sato, H., Kogure, T., Yamagishi, A., Kawamata, J.; *Chem. Commun.*, **2009**, 45, 6964.

(14) Verbiest, T., Elshocht, S.V., Persoons, A., Nuckolls, C., Philips, K.E., Katz, T.J.; *Langmuir*, **2001**, 17, 4685.

(15) Sioncke, S., Verbiest, T., Persoons, A.; *Mater. Sci. Eng., R.*, **2003**, 42, 115.

(16) Kleinman, D.A.; *Phys. Rev.*, **1962**, 128, 1761.

(17) Jerphagnon, J., Kurtz, S.K.; *J. Appl. Phys.*, **1970**, 41, 1667.

(18) Kawamata, J., Inoue, K., Inabe, T.; *Appl. Phys. Lett.*, **1995**, 66, 3102.

(19) Reinhardt, B.A., Brott, L.L., Clarson, S.J., Dillard, A.G., Bhatt, J.C., Kannan, R., Yuan, L., He, G.S., Prasad, P.N.; *Chem. Mater.*, **1998**, 10, 1863.

# Chapter 3 Factors for Enhancing the Two-Photon Absorption Cross-Section of Organic Compounds Hybridized with Inorganic Layered Compounds

## 3-1 Introduction

Among several possible explanations[1] to explain enhancements in the two-photo absorption cross-section described in section 5 of chapter 1, this study focused on two factors: (2) improved molecular orientation and (3) extension of the π-conjugated systems due to the improved planarity of the dyes. The contributions of these factors to $\sigma^{(2)}_{peak}$ were quantitatively investigated by employing four dyes. Among the two factors, the former should be observed from all of the clay/dye composite films fabricated by the protocol described in chapter 2, because the composites are definitely stacked in layer-by-layer mode in the film. On the other hand, for composites consisting of dyes whose planarity should be improved by the intercalation, such as MPPBT, not only the former effect but also the latter effect should be observed. Therefore, spectroscopic properties both in solution and in films of dyes whose planarity are thought not to be improved were compared with those of dyes whose planarity should be improved by the intercalation. As for former group of dyes, we selected FL and PIC. The latter group of dyes selected in this study were MPPBT and TMPyP, as was already described in chapter 1.

## 3-2 One Photon Absorption Properties - Dispersion and Film -

Considerable solvatochromism is often seen for efficient TPA compounds (see for example reference 2). Thus, prior to discussing the electronic properties of clay/dye composites, we examined the solvatochromic behavior of all the dyes treated in this study. The solvatochromic behaviors of the dyes were investigated by measuring the UV-vis absorption spectra in water, ethanol, DMSO, acetone and chloroform. The wavelengths of the absorption maxima ($\lambda_{max}$) and molar absorption coefficients at the $\lambda_{max}$ of the dyes dissolved in those solvents are summarized in Table 3-1, together with the polarity parameters[3] ($E_T(30)$) of the solvents. The $\lambda_{max}$ of MPPBT, FL and PIC tended to red-shift as the $E_T(30)$ of the solvent decreased. The value of the molar absorption coefficients at the $\lambda_{max}$ of dyes tended to increase with decreasing $E_T(30)$ of solvents. On the other hand, the $\lambda_{max}$ of TMPyP was almost constant when the solvent was varied. However, the molar absorption coefficients tended to increase as the $E_T(30)$ decreased. Such solvatochromic behaviors are typical of compounds exhibiting positive solvatochromism.

UV-vis spectra of homogenous solution of MPPBT, TMPyP, FL and PIC and the dispersion of the composites with SSA are shown in Figure 3-1. As was described in chapter 2, dispersions of SSA/MPPBT and SSA/FL composites were fabricated by mixing water dispersion of SSA and

**Table 3-1** Absorption maxima ($\lambda_{max}$) and molar absorption coefficient of dyes in various solvents. The polarity parameters ($E_T(30)$) of the solvents are also shown.

| Solvents | $E_T(30)$ | $\lambda_{max}$ (nm) | | | | Molar absorption coefficients ($\times 10^3$ L mol$^{-1}$ cm$^{-1}$) | | | |
|---|---|---|---|---|---|---|---|---|---|
| | | MPPBT | TMPyP | FL | PIC | MPPBT | TMPyP | FL | PIC |
| Water | 63.1 | 453 | 423 | 420 | 523 | 66.3 | 226 | 43.4 | 64.0 |
| Ethanol | 51.9 | 465 | 424 | 430 | 524 | 70.4 | 228 | 59.0 | 75.4 |
| DMSO | 45.1 | 466 | 424 | 429 | 525 | 66.0 | 276 | 63.9 | 70.5 |
| Acetone | 42.2 | 462 | 422 | 427 | 524 | 70.8 | 233 | 61.7 | 74.0 |
| Chloroform | 39.1 | insoluble | insoluble | 445 | 529 | insoluble | insoluble | 59.4 | 75.0 |

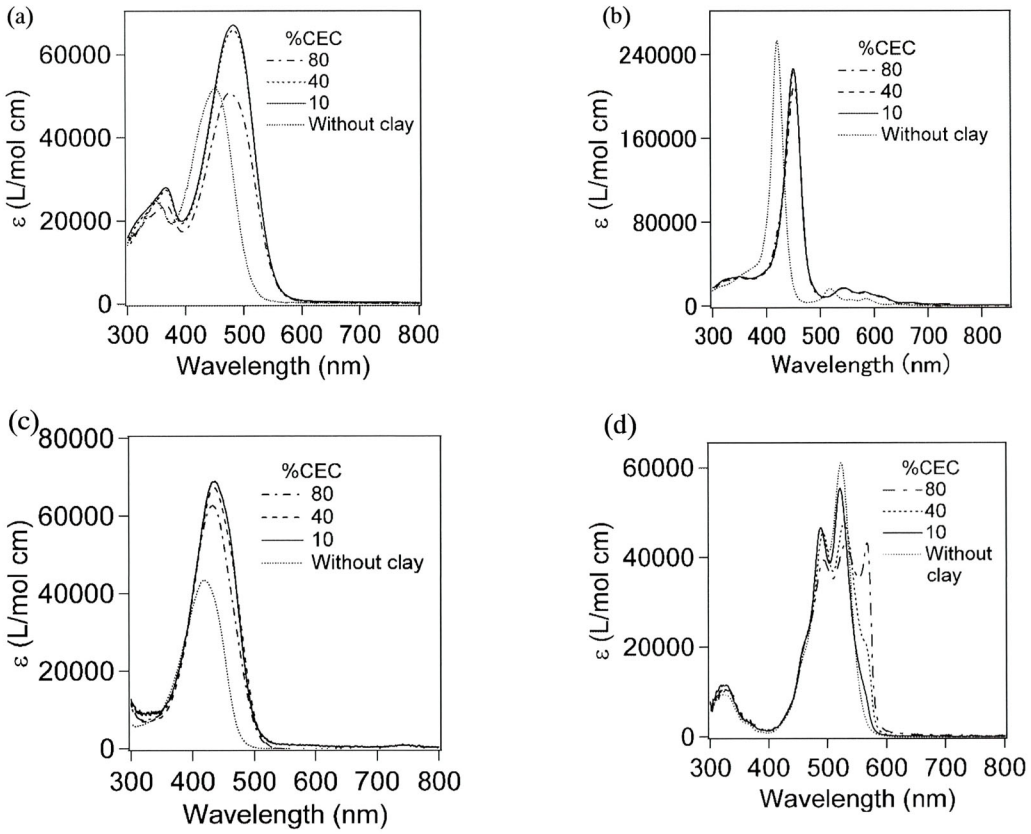


**Figure 3-1** Absorption spectra of (a) MPPBT, (b) TMPyP, (c) FL and (d) PIC in dispersions of composites with SSA prepared at various %CEC and in water (TMPyP and PIC) and a dimethylsulfoxide (0.5% v/v)-water mixed solvent (MPPBT and FL).

DMSO solution of MPPBT or FL. Therefore, differences in absorption spectra of the dyes observed for an homogeneous DMSO solution and the dispersion of the composites were attributed not only due to a change of environment of dyes related to the adsorption onto SSA, but also due to solvatochromism. In order to distinguish the two possible causes of the spectral differences, spectra of homogeneous solutions of MPPBT and FL were recorded in DMSO-water mixed solvents with the same mixture ratio as those of the dispersions. As for the absorption spectra of the dispersions themselves, composites prepared at 10%, 40% and 80% CEC have been provided in the figures. The respective wavelengths of the absorption maxima of dyes are summarized in Table 3-2. The absorption maxima of composite dispersions of MPPBT, TMPyP and FL showed spectral shifts to longer wavelength compared to those of homogeneous solutions of these dyes. This clearly indicates

that MPPBT, TMPyP and FL molecules in dispersion interacted with SSA. Namely, these dyes adsorb onto the surfaces of clay layers through an ion-exchange reaction when mixed with an SSA dispersion.

In contrast to the cases of MPPBT, TMPyP and FL, an obvious spectral shift of the absorption maxima of the main absorption band between homogeneous solution and composite dispersion was not observed for PIC. However, a growth with increasing %CEC of an additional absorption band at a peak wavelength of 567 nm can be seen in the absorption spectra of SSA/PIC composites (Figure 3-1 (d)). This spectroscopic difference between homogeneous solution and composite dispersion clearly indicates the adsorption of PIC onto SSA in dispersion. It is reported that PIC forms J-aggregates when PIC adsorbs onto the surface of clay at a high %CEC[4]. Therefore, owing to the formation of J-aggregate, the additional absorption band was thought to be appeared. Nonlinear optical properties of aggregated dyes are known to be significantly different from those of dyes in a disaggregated state[5,6]. A consideration of the properties of dyes in the J-aggregated state is interesting. However, hereafter the discussion of SSA/PIC composites prepared at %CEC's of higher than 40% has been excluded, because the aim of this paper is the comparative study of TPA properties of dyes obtained by simple formation of a composite with SSA.

An increase of the %CEC produced blue-shifts of absorption bands in spectra of composite dispersions of SSA/MPPBT and SSA/FL, though no %CEC dependence was observed for SSA/TMPyP composite dispersion. For most of cationic dyes adsorbed on a clay surface at a high %CEC, H-aggregates are typically formed[7], which are accompanied by blue-shifts of absorption bands[7,8]. On the other hand, TMPyP is known as a dye which adsorbs on SSA without aggregation even at a loading of 100%[9] Therefore, the most likely reason for the blue-shift observed for the SSA/MPPBT and SSA/FL composite dispersion at the high %CEC is the formation of H-aggregates.

**Table 3-2** Wavelengths of absorption maxima (nm) of dyes in homogeneous solution, in composite dispersion and composite films

| | | MPPBT | TMPyP | FL | PIC |
|---|---|---|---|---|---|
| in homogeneous solution | | 466 (in DMSO-water mixed solvent) | 420 (in water) | 420 (in DMSO-water mixed solvent) | 523 (in water) |
| in dispersion | 10 %CEC | 482 | 448 | 435 | 521 |
| | 20 | 482 | 448 | 435 | 523 |
| | 40 | 482 | 448 | 435 | - |
| | 60 | 482 | 448 | 435 | - |
| | 80 | 476 | 448 | 432 | - |
| in composite film | 10 %CEC | 505 | 479 | 444 | 524 |
| | 20 | 500 | 478 | 444 | 525 |
| | 40 | 486 | 475 | 440 | - |
| | 60 | 479 | 468 | 436 | - |
| | 80 | 472 | 460 | 436 | - |

Next, let us focus on the topics of the optical properties of dyes in hybrid film. UV-vis spectra of SSA/MPPBT, SSA/TMPyP, SSA/FL and SSA/PIC films are shown in Figure 3-2. Absorption spectra of films consisting of composites prepared at 10%, 40% and 80% CEC are provided in the figure. In all cases, the $\lambda_{max}$ of dyes in hybrid films were longer than those in dispersions prepared at the same %CEC. Dyes in the films should be surrounded by hydrophobic Si-O-Si networks, whereas dyes in composite dispersions should contact water on at least one side of molecule. As described, positive solvatochromic MPPBT, FL and PIC show red-shifts of absorption bands when these molecules are placed in a hydrophobic environment. Therefore, a hydrophobic environment in the films should lead to red-shifts of absorption bands for MPPBT, FL and PIC. Although solvatochromism was not observed for TMPyP in homogeneous solution, as well as other dyes, $\lambda_{max}$ of the soret band of TMPyP in the composite films were longer than those in dispersions. Similar red-shifts of the soret band compared to dispersion was also reported by Takagi et. al. for

freeze-dried composite films of TMPyP and SSA[9]. These larger bathochromic shifts of the Soret band were explained by a stronger flattening of the porphyrin molecules due to the confinement of TMPyP in the 2-dimensional space between clay layers[9-11]. The red-shifts observed for MPPBT and TMPyP, in which planarity were thought to be improved by film formation, were larger than those of FL and PIC, in which planarity in the film were thought to be similar to that in solution. For example, in the case of 10% CEC, the shifts of $\lambda_{max}$ of MPPBT and TMPyP were 39 and 59 nm, respectively, whereas those of FL and PIC were 24 and 1 nm, respectively. These facts suggest that planarity of MPPBT and TMPyP are improved in the film. Except for PIC, which forms J-aggregates, the $\lambda_{max}$ of the films were found to blue-shift as the %CEC increased. In dispersions,blue-shifts of $\lambda_{max}$ due to the formation of H-aggregates were found for MPPBT and FL when %CEC was higher than 80%. However, in the films, blue-shifts were observed even when the spectra of films of 10% and 20% CEC were compared. One of the most probable reasons of this blue-shift is formation of H-aggregates. Even for TMPyP which is known to adsorb onto a clay surface without aggregation up to 100% CEC in dispersions, the formation of small amount of H-aggregate in the film has been reported when the %CEC is only 8%[9]. As another reason of the blue-shifts of MPPBT and TMPyP, insufficient flattening of the π-electron system at a higher %CEC might be considered, because large numbers of molecules accommodated in the interlayer space might result in an extended interlayer spacing. Therefore, in the next section, the interlayer spacings of the films obtained by X-ray diffraction (XRD) measurements will be discussed.

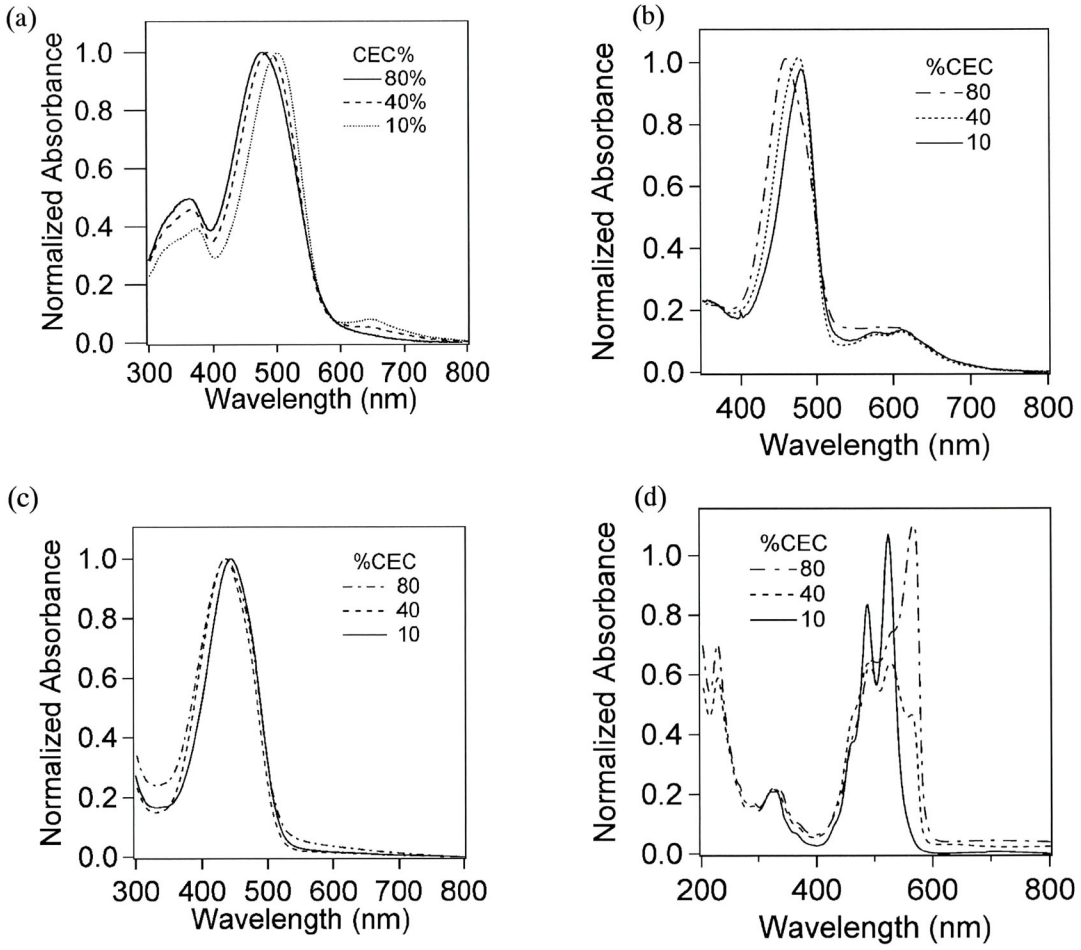


**Figure 3-2** Absorption spectra of films of (a) MPPBT, (b) TMPyP, (c) FLand (d) PIC fabricated from composites with SSA prepared 10%, 40% and 80% CEC.

## 3-3 Interlayer Spacing of the Composite Films

The obtained XRD patterns of SSA/MPPBT and SSA/TMpyP composite films are shown in Figure 3-3. The interlayer spacing of the MPPBT film was found to increase when the %CEC was higher than 40%, whereas that of TMPyP was almost constant, even when %CEC reached to 100%. In order to understand the difference, the coverage, which is defined as the percentage of SSA surface covered with dyes, has been analyzed. In concrete terms, coverage can be calculated from following equation:

$$\text{Coverage (\%)} = \frac{\text{\%CEC} \times \text{Cross-sectional area of a dye per cationic moiety}}{\text{Surface area of SSA per one anionic site}}$$

Molecular sizes and valences are different between MPPBT and TMPyP. Therefore, even at the same %CEC, the coverage should be different depending on the guest molecule. Cross-sectional areas of MPPBT and TMPyP viewed from normal direction of the π-electron system, under the assumption that the π-electron systems of them are flattened completely, were estimated to be about 3.5 and 2.5 $nm^2$. The cross-sectional areas of MPPBT and TMPyP per cationic moiety were

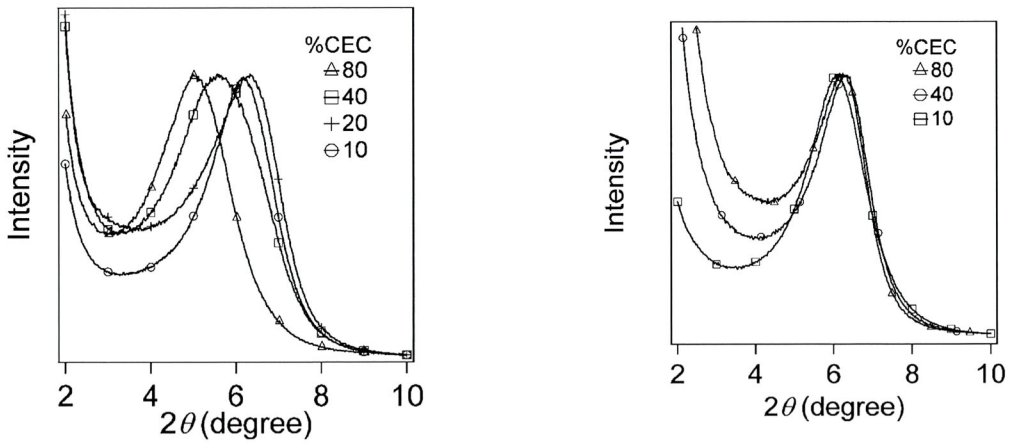


**Figure 3-3** X-ray diffraction patterns of (a) SSA/MPPBT and (b) SSA/TMPyP films fabricated from composites prepared at various %CEC.

calculated to be 1.8 and 0.6 $nm^2$, respectively, because MPPBT is a divalent and TMPyP is a tetravalent cations. This fact indicates the coverage of MPPBT on a SSA surface should be 3 times higher than that of TMPyP even at the same %CEC. The calculated surface area of SSA per one anionic site is 1.3 $nm^2$. Interlayer spacings of the films as the function of the coverage have been plotted in Figure 3-4. When the coverage were smaller than 50%, the interlayer spacing coincided with the summation of the thickness of SSA and molecular thicknesses, estimated under the assumption that the molecules were completely flattened. This fact suggests MPPBT and TMPyP are flattened in between SSA layers at a lower coverage. Since both sides of a SSA layer is covered with dyes, the space filling percentage of the interlayer space of the films formed by stacking of composites with 50% coverage should be 100% (see Figure 3-5(b)). Therefore, when the coverage is smaller than 50%, molecules can be accommodated parallel to SSA layer in the interlayer space in monolayer mode (see Figure 3-5(a)). However, when the coverage were higher than 50%, monolayer mode accommodation of dyes should be no longer possible and the dye molecules are thought to be tilted to the plane of SSA (see Figure 3-5(c)). If the dyes were homogeneously adsorbed onto clay layer completely, the models shown in Figure 3-5 (b) can be applied to the obtained film. However,

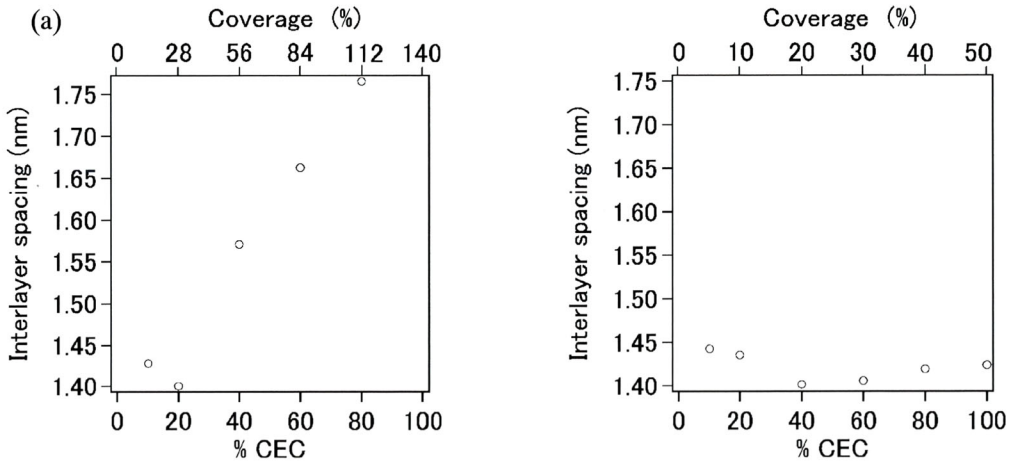


**Figure 3-4** Interlayer spacing of (a) SSA/MPPBT and (b) SSA/TMPyP composite films depending on surface coverage.

adsorption of dyes onto a clay surface is not always homogeneous and the space filling percentage could exceed 100% in some regions, even when averaged coverage was smaller than 50%. Reflecting this, the interlayer spacing of a SSA/MPPBT film increased with an increase in the coverage when the coverages were higher than about 40%. In this situation, the dye molecules are not necessarily flattened. Thus, for SSA/MPPBT films fabricated from composites prepared at a high %CEC, not only the formation of H-aggregates, but also incomplete flattening is a possible reason for the blue-shift of the absorption band. On the other hand, the coverage of the SSA/TMPyP composite was smaller than 50% even at 100% CEC. Reflecting this, the interlayer spacing of a SSA/TMPyP film was almost constant until 100% CEC. Therefore, π-electron system of TMPyP in the film should be completely flattened even at 100% CEC. Thus, the blue-shift of the absorption band found from a SSA/TMPyP film fabricated at a high %CEC was likely to be solely due to the formation of H-aggregates.

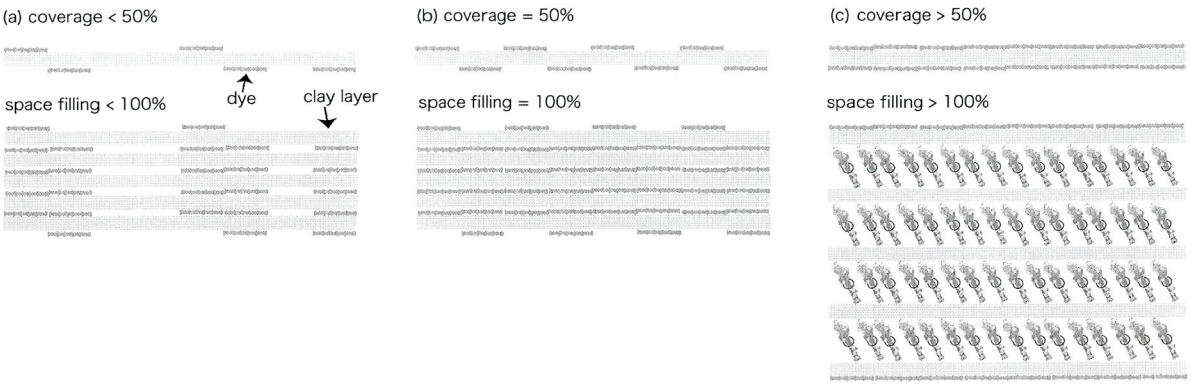


**Figure 3-5** Schematic representation of relationship between coverage and space filing percentage., (a) smaller coverage than 50%, (b) coverage of 50%, (c) coverage higher than 50%.

## 3-4 Two-Photon Absorption Properties

TPA spectra of DMSO solution and composite films of MPPBT, TMPyP, FL and PIC are shown in Figure 3-6, and $\sigma^{(2)}_{peak}$ values are summarized in Table 3-3. Since the dyes were not dissolved in water at a concentration high enough for Z-scan measurements, measurements of homogeneous solution were made using DMSO solution of dyes with the concentration of $2 \times 10^{-3}$ mol $l^{-1}$. Composite films, except for a 10% CEC SSA/PIC composite film, were fabricated by filtering a composite dispersion containing the same amount of SSA prepared at the optimized condition as described in Section 3 of Chapter 2. Since the optimized concentration of clay in dispersions with 10% CEC were higher than those of 80% CEC, 10% and 80% CEC films were fabricated by filtering 20 and 160 ml of composite dispersions, respectively. The $\sigma^{(2)}_{peak}$ of PIC in 10% CEC composite films was considerably smaller than those of the other dyes. Therefore, in order to increase the number of molecules in the optical path, a film fabricated by filtering 100 ml of composite dispersion was employed for the Z-scan measurement.

Several dyes exhibited very large values of $\sigma^{(2)}$ at the double resonance regions (near the cut-off wavelengths of OPA bands). However, in this paper, discussion is mainly focused on $\sigma^{(2)}_{peak}$, because the main aim of this study is to compare the TPA properties of dyes inside and outside of the interlayer spaces of SSA and this can be discussed more clearly in terms of the lowest-energy TPA transitions ($\sigma^{(2)}_{peak}$).

Comparing the $\sigma^{(2)}_{peak}$ of dyes in composite films and those in DMSO solution, enhancements of $\sigma^{(2)}_{peak}$ observed for FL and PIC, whose planarities are thought to be almost the same both in composite films and in DMSO solutions, were 1.7 and 3 times, respectively, at a %CEC of 10%. It is reported that the $\sigma^{(2)}_{peak}$ is increased 1.9 times by improved orientation owing to the intercalation[1,12]. Considering the experimental error, the enhancement of $\sigma^{(2)}_{peak}$ of FL by the intercalation can be explained by improved molecular orientation. However, the enhancement of $\sigma^{(2)}_{peak}$ observed for PIC

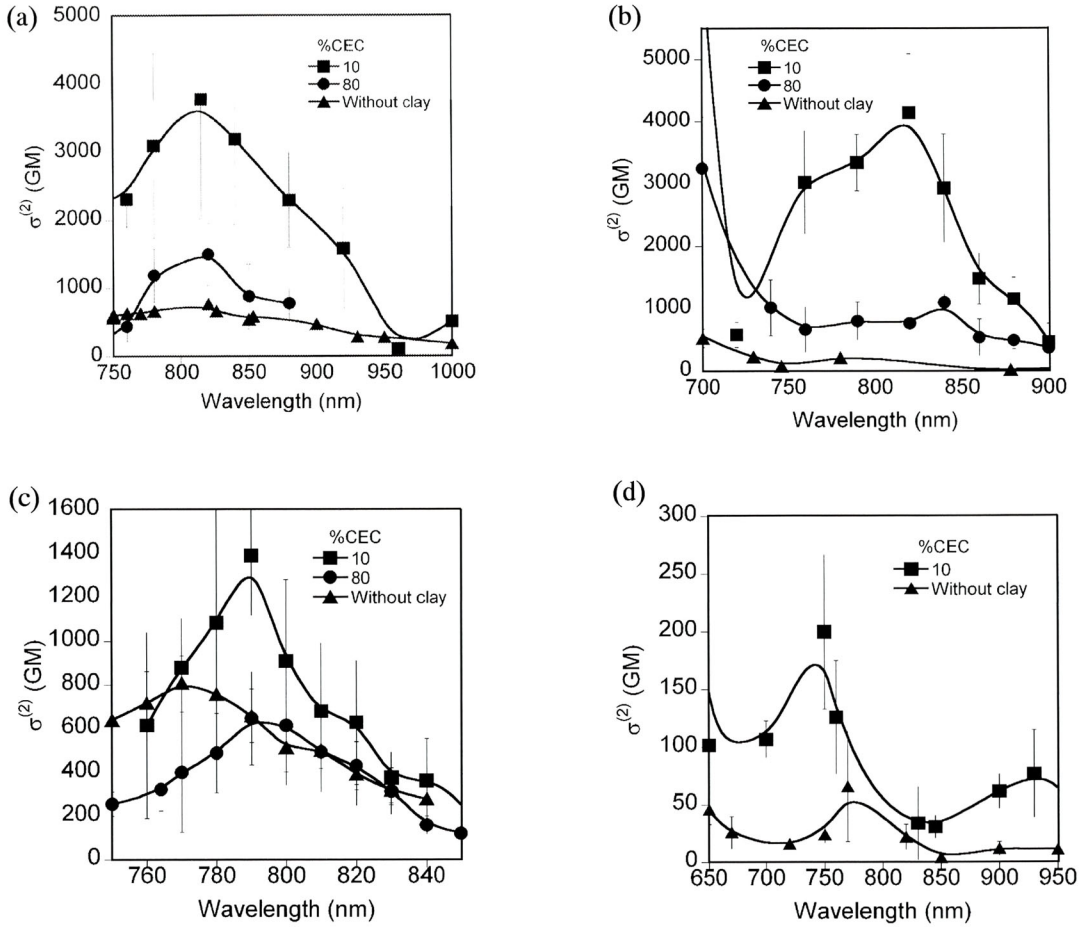


**Figure 3-6** TPA spectra of (a) MPPBT, (b) TMPyP, (c) FL and (d)PIC in DMSO and in composite films.

was somewhat larger than that expected only from the improved molecular orientation. The $\sigma^{(2)}_{peak}$ is known to be increased up to 2 times when the dyes are placed in significantly hydrophobic environments[2]. The excess enhancement of the $\sigma^{(2)}_{peak}$ of PIC was thought quite likely to arise from the hydrophobic environment provided by the interlayer space of SSA.

Much more drastic enhancements were observed for MPPBT and TMPyP. The $\sigma^{(2)}_{peak}$ of MPPBT and TMPyP in the composite films fabricated at 10% CEC were 5.1 and 13 times as large as those in DMSO solution, respectively. For those dyes, improvements of planarity of the π-conjugated system were expected from the intercalation. Therefore, not only the enhancement due to the improved molecular orientation but also that due to the improved planarity of the π-conjugated system can be

**Table 3-3** $\sigma^{(2)}_{peak}$ (GM in unit) of MPPBT, TMPyP, FL and PIC in homogeneous DMSO solution and in composite films fabricated from composites prepared at 10% and 80% CEC

| | | MPPBT | TMPyP | FL | PIC |
|---|---|---|---|---|---|
| in homogeneous DMSO solution | | 770 | 300 | 810 | 66 |
| in composite films | 10% CEC | 3900 | 4000 | 1400 | 200 |
| | 80 | 1500 | 1000 | 720 | - |

expected. Here, let us consider the extent of enhancement of $\sigma^{(2)}_{peak}$ expected from the improved molecular planarity. The increase of $\sigma^{(2)}_{peak}$, expected simply due to the extension of the π-conjugated system, were estimated using an equation proposed by Moreno et. al[13]. In solution, the diacetylene moiety of MPPBT is rotated around the axis by a torsional motion. Therefore, the π-conjugated system of MPPBT in solution was assumed to be divided at the center of the diacetylene moiety into two independent parts containing the styrylpyridyl group, whereas that in the composite film is completely conjugated over the whole molecule because a flattened π-conjugated system was expected for MPPBT in the film. The $\sigma^{(2)}_{peak}$ of MPPBT in the film, calculated on thisassumption was 2 times as large as that in solution. In this estimation, we neglected electronic communication between the distorted rings. However, it is reported for MPPBT that some electronic communication through the triple bond is still maintained throughout the molecule even when the rings are perpendicularly connected[1]. Therefore, the evaluated enhancement of MPPBT could have been somewhat overestimated. A similar evaluation was also made for TMPyP. In solution, the four pyridine rings of TMPyP are reported to be orthogonal to the central porphyrin ring[9-11]. Therefore, the π-conjugation of each ring is thought to be independent. On the other hand, the rings in films of TMPyP are thought to be coplanar. This assumption is supported by references 9-11 and our XRD result described above. Therefore, the π-electron system of TMPyP in the film should be conjugated over the whole molecule. The calculated $\sigma^{(2)}_{peak}$ of TMPyP in the film based on this model was 3.4 times as large as that in solution.

As mentioned previously, considerable red-shifts of one-photon absorption bands were observed for MPPBT and TMPyP when the dyes were intercalated in SSA layers. Consequently, the detuning energies of intercalated MPPBT and TMPyP should be smaller than those in solution. Therefore, the magnitudes of enhancements of $\sigma^{(2)}_{peak}$ attributed by to reduction of the detuning energy accompanied by the red-shifts of absorption bands[14-16] observed for MPPBT and TMPyP films fabricated at 10% CEC have been estimated. One- and two-photon absorption maxima of MPPBT in DMSO solution were 455 and 800 nm (2.72 and 1.55 eV), respectively. Thus the detuning energy, the energy difference between the energy of the photon used for two-photon excitation and the energy gap between ground and excited states, of MPPBT in DMSO was calculated to be 1.17 eV. On the one hand, one- and two-photon maxima of MPPBT in the film were 502 and 820 nm (2.47 and 1.51 eV), respectively. Therefore, the detuning energy of MPPBT in the film was estimated to be 0.96 eV. Since $\sigma^{(2)}_{peak}$ is proportional to the square of the inverse of the detuning energy, the estimated enhancement of $\sigma^{(2)}_{peak}$ of MPPBT due to the decrease of the detuning energy was 1.5 times. A similar estimation was also made for TMPyP. One- and two-photon absorption maxima of TMPyP in DMSO solution were 422 and 840 nm (2.94 and 1.58 eV), and those in film were 482 and 830 nm (2.57 and 1.49 eV), respectively. Therefore, the enhancement of $\sigma^{(2)}_{peak}$ of TMPyP attributed to the decrease of the detuning energy accompanied by film formation was calculated to be 1.8 times.

When the three factors, improved molecular orientation, extension of the π-conjugated system and decrease of the detuning energy, were multiplied together, the estimated enhancements of $\sigma^{(2)}_{peak}$ of MPPBT and TMPyP were 5.7 and 11 times, respectively. Those values showed good agreement with experimental values of 5.1 and 13 times. However, in the case of MPPBT, the factor due to the extension of the π-conjugated system has been overestimated. The overestimation of MPPBT was likely to be compensated by the factor obtained by incorporating it into the hydrophobic interlayer

space of the clay mineral.

The $\sigma^{(2)}_{peak}$ observed from films fabricated at 80% CEC were smaller than those fabricated at 10% CEC. The primary reason of this diminishment is probably the formation of H-aggregates, because the formation of H-aggregate is known to suppress the nonlinear optical response of molecules[17]. In the case of MPPBT, incomplete flattening of dyes suggested by the XRD results may be an additional reason. Therefore, in order to enhance $\sigma^{(2)}_{peak}$ of dyes sufficiently in the films, %CEC must be kept low so as to suppress the formation of H-aggregates. This limitation of chromophore density might be a disadvantage of the present composite. However, even at the 10% CEC level where the formation of H-aggregates was practically negligible, the concentration of a dye, for example, MPPBT, in the film was calculated to be $10^{-1}$ mol $l^{-1}$. This concentration is considerably higher than that of a saturated solution of a conventional dye. Thus, it is concluded that the present composite films are attractive TPA materials from the view points of both the enhanced $\sigma^{(2)}_{peak}$ and the high density of chromophores in the sample.

It should be noted here that the spectroscopic features of the obtained film were suitable for TPA applications, such as 3D optical-data storage, where solid materials are required. The 3D optical-data storage market is one of the most important applications of the TPA materials because of its large size. Figure 3-7 shows TPA spectra including the double resonance regions of SSA/MPPBT and SSA/TMPyP films fabricated from composites prepared at 10% CEC. Considerable enhancements of $\sigma^{(2)}$ were observed in those regions, with the maximum values of $\sigma^{(2)}$ of MPPBT and TMPyP of 13000 and 11000 GM, respectively. The values at a wavelength near 680 nm, which is the wavelength used for DVD recording, were as large as that expected to be attained later than 2015 in the 2007 road-map of the Ministry of Economy, Trade and Industry. Thus the present films might break a bottleneck in 3D optical-data storage technology.

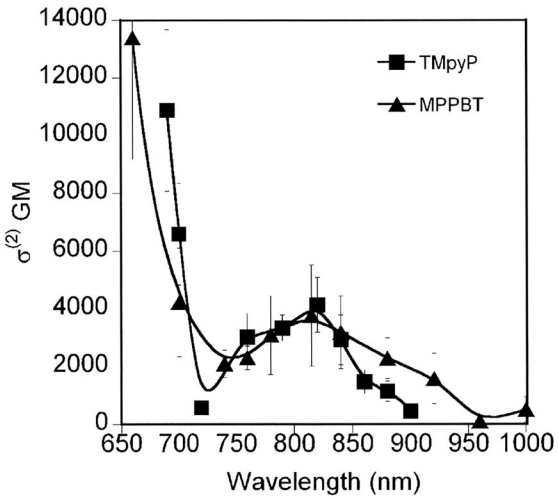


**Figure 3-7** TPA spectra of SSA/MPPBT and SSA/TMPyP films fabricated from composites prepared at 10% CEC.

## 3-5 Conclusion

One- and two-photon absorptions, and XRD measurements of transparent and oriented composite films consisting of MPPBT, TMPyP, FL or PIC, and SSA at various %CEC values were conducted so as to understand the factors that enhance $\sigma^{(2)}_{peak}$ of dyes in the interlayer space of SSA. As a result, when the dyes are intercalated in clay films fabricated by the present protocol, the $\sigma^{(2)}_{peak}$ of all the dyes have been found to be enhanced because of (2) the π-plane of the molecules and the direction of electric field of incident light lie in the same plane and, occasionally, because of (4) the hydrophobic environment of the interlayer space of clay minerals,. The $\sigma^{(2)}_{peak}$ of dyes in the present films, enhanced by the two above factors, were from two to three times larger than that in solution. Much more drastic enhancement of $\sigma^{(2)}_{peak}$ was observed from dyes of which planarity was improved by incorporating into the interlayer space of the clay mineral. For such dyes, not only the factors (2) and (4), but also the factors, (3) extension of the π-conjugated system due to the improved planarity and the resulting (5) decrease of the detuning energy, were effective contributors to the enhancements of $\sigma^{(2)}_{peak}$. The enhancements of $\sigma^{(2)}_{peak}$ were significant when the %CEC was kept small enough so as to suppress the formation of H-aggregates. The $\sigma^{(2)}_{peak}$ of TMPyP in the film fabricated from composites prepared at 10% CEC was found to be enhanced up to 13 times as large as that in solution.

Similar situations should be obtained in hybrid materials consisting not only of clay minerals but also of other inorganic layered compounds. Furthermore, mesoporous materials such as zeolites chould be utilized as the host materials, because such mesoporous materials can also confine dyes as well as inorganic layered materials. In this study SSA, a smectite clay mineral was employed as a prototypical inorganic layered host material. SSA does not have any photo-functionalities and does not have a significant influence on the electronic properties of the guest molecules. However, if photo-functional compounds are employed as the host materials, unique TPA materials utilizing

functionalities not only of the guests, but also of the host materials, might be obtained.

The confinement obtained in the interlayer space of inorganic layered materials may be utilized to enhance $\sigma^{(2)}_{peak}$ of molecules possessing very large π-conjugated system. As mentioned in Section 3 of Chapter 1, there is a limitation in the enhancement of $\sigma^{(2)}_{peak}$ from an of the extension of the π-electron system due to the difficulty in maintain the planarity of a large π-electron system. However, improved of the planarity of a large π-electron system obtained confinement in inorganic layered materials may provide a solution to this problem. Thus, it is concluded that the hybridization of dyes with layered inorganic materials is a promising means for obtaining promising TPA materials.

## References


(1) Kamada, K., Tanamura, Y., Ueno, K., Ohta, K., Misawa, H.; *J. Phys. Chem. C*, **2007**, 111, 11193.

(2) Woo, H.Y., Liu, B., Kohler, B., Korystov, D., Mikhailovsky, A., Bazan, G.C.; *J. Am. Chem. Soc.*, **2005**, 127, 14721.

(3) Reichardt, C.; *Chem. Rev.*, **1994**, 94, 2319.

(4) Ogawa, M., Kawai, R., Kuroda, K.; *J. Phys. Chem.*, **1996**, 100, 16218.

(5) Collini, E., Ferrante, C., Bozio, R.; *J. Phys. Chem. C*, **2007**, 111, 18636.

(6) Wang, Y.; *Chem. Phys. Lett.*, **1986**, 126, 209.

(7) Bujdak, J., Iyi, N.; *J. Coll. Interface Sci.*, **2008**, 326, 426.

(8) Kawamata, J., Hasegawa, S.; *J. Nanosci. Nanotechnol.*, **2006**, 6, 1620.

(9) Takagi, S., Shimada, T., Eguchi, M., Yui, T., Yoshida, H., Tryk, D.A., Inoue, H.; *Langmuir*, **2002**, 18, 2265.

(10) Chernia, Z., Gill, D.; *Langmuir*, **1999**, 15, 1625.

(11) Kuykendall, V.G., Thomas, J.K.; *Langmuir*, **1990**, 6, 1350.

(12) Suzuki, Y., Nakagawa, K., Nishioka, Y., Tenma, Y., Kawamata, J.; *Clay Science*, **2010**, 14, 229.

(13) Moreno, J., Kuzyuk, M.; *J. Chem. Phys.*, **2005**, 123, 194101.

(14) Rumi, M., Ehrlich, J.E., Heikal, A.A., Perry, J.W., Barlow, S., Hu, Z., McCord-Maughon, D., Parker, T.C., Rockel, H., Thayumanavan, S., Marder, S.R., Beljonne, D., Bredas, J.L.; *J. Am. Chem. Soc.*, **2000**, 122, 9500.

(15) Kamada, K., Ohta, K., Iwase, Y., Kondo, K.; *Chem. Phys. Lett.*, **2003**, 372, 386.

(16) Hirakawa, S., Kawamata, J., Suzuki, Y., Tani, S., Murafuji, T., Kasatani, K., Antonov, L., Kamada, K., Ohta, K.; *J. Phys. Chem. A*, **2008**, 112, 5198.

(17) Carpenter, M.A., Willand, C.S., Penner, T.L., Williams, D.J., Mukamel, S.; *J. Phys. Chem.*, **1992**, 96, 2801.

# Chapter 4 Conclusion

This study established a novel protocol for fabricating low light-scattering clay/dye composite films with a definite layer-by-layer stacking structure. Through the use of these films, the reasons why the $\sigma^{(2)}_{peak}$ of dyes were drastically enhanced in the composite consisting of inorganic-layered-compound/dye compared to those in solution have been clarified.

Typical clay/dye composite are light-scattering media and the component molecules are in random orientation. The difficulty in fabricating extremely low light-scattering composites suitable for characterizing the linear- and nonlinear-optical properties of dyes in a composite have hindered spectroscopic studies of such composites. Furthermore, the random orientation of the dyes in the composites limited the photo-functional activities of the composites. This study has solved these problems and opened a way to use such composite for optical applications. By using the present protocol, composite films can be fabricated even when a variety of organic dyes and inorganic layered compound are desired to be employed. This has extended the use of organic compounds as optical materials. Organic compounds are attractive as photo-functional materials because of their salient efficiencies and fast responses. However, organic materials which satisfy the requirements for optical devices were practically limited to single crystals. Growth of organic single crystals is not easy and is difficult to apply in industrial processes. The composite films fabricated in this study are a new class of organic based optical materials obtainable through a simple procedure.

The reasons why the $\sigma^{(2)}_{peak}$ of dyes were enhanced in the composite have been clarified using films fabricated by the present protocol. One- and two-photon absorptions, and XRD measurements were conducted so as to characterize dyes in the interlayer space of SSA. As a result, $\sigma^{(2)}_{peak}$ of all the dyes was found to be enhanced because of (2) the $\pi$-plane of the molecules and the direction of electric field of incident light lie in the same plane. Further enhancements of $\sigma^{(2)}_{peak}$ of some dyes were found to be due to other reasons: (3) extension of the $\pi$-conjugated system due to the improved

planarity, (4) the hydrophobic environment of the interlayer space of clay minerals, and (5) a decrease of the detuning energy. The correct selection of dyes which are expected to maximize the factors (3)-(5) was found to be the prime requirement to effect the design of composites exhibiting efficient values of $\sigma^{(2)}_{peak}$. The present design strategy of efficient TPA materials, which maximizes the potential optical nonlinearities of dyes, is totally different from previous ones which were mainly focused on structural modification of organic molecules. A combination of the present and previous design strategies should result in the production of next-generation efficient TPA materials.

This study has provided a means for fabricating efficient solid state TPA materials. The materials obtained have enabled TPA induced excitation even when a newly developed compact and cheap intense pulsed laser is used as the light source. Furthermore, the features of the obtained films were suitable for TPA applications where solid samples are required, such as 3D optical-data storage, which is one of the most attractive applications of such materials because of the large commercial market. Thus it is concluded that the formation of composite film by employing the present film fabrication protocol should be a promising strategy for obtaining efficient TPA materials.

# Appendix

## Measurement

### UV-visible-near infrared absorption and transmittance spectra measurements

Absorption spectra of solution and dispersion of composites with dye concentrations of $10^{-5}$ M were measured with JASCO Model U-670 spectrometer using 10 mm quartz cuvettes. Absorption spectra of films were measured using the same spectrometer equipped with an attachment for films (JASCO, VTA-752).

### Two-photon absorption measurement

TPA spectra were obtained by plotting TPA cross sections ($\sigma^{(2)}$) at respective wavelengths measured by the open-aperture Z-scan technique[1]. A femtosecond pulsed beam from an optical parametric amplifier (Spectra-Physics, OPA-800C) driven by a beam from a regenerative amplifier (Spectra-Physics, Spitfire) was used as the light source. The typical pulse duration was 150-200 fs with a repetition rate of 1 kHz. The incident beam was focused by a plano-convex lens ($f$ = 150 mm) and the sample was scanned along the propagation axis of the incident beam. Average incident power was varied from 0.01 to 0.4 mW, corresponding to on-axis peak powers ($I_0$) of 6-240 GW $cm^{-2}$. Proportionality relations between the TPA absorbance, $q_0$, and the incident power, and hence $I_0$, was confirmed at each measurement. The proportionality relation is reliable evidence that the transmittance changes observed from the Z-scan measurements were due purely to TPA and any other NLO processes that could pile up in the Z-scan patterns were not observed[2,3].

For the Z-scan measurements of homogeneous solutions, the sample must satisfy two requirements. One is the thickness of the sample. This must be smaller than the Rayleigh length. The Rayleigh length of the optical setup used for the present study was varied depending on the

wavelength from 2 to 4 mm. Therefore, two types of optical cells with thicknesses of 1 and 2 mm were selected depending on the Rayleigh length. The other requirement is the optical density of the sample. For reliable measurements, optical density, and thus the concentration of the solution, must be higher than $10^{-3}$ mol $l^{-1}$ when the expected $\sigma^{(2)}$ is 100 GM. Therefore, solutions with aconcentration of $10^{-2}$ - $10^{-3}$ mol $l^{-1}$ were employed for all the Z-scan measurements. There is a possibility that the organic compounds form H- or J- aggregates in such a high-concentration solution. Therefore, one-photon absorption spectra of the concentrated solutions were compared to those observed for dilute ($10^{-6}$ mol $l^{-1}$) solutions. However, no meaningful difference was observed. Therefore, the TPA cross-sections of solutions measured in this study were considered to be the values of the monomer.

**X-ray diffraction measurement**

X-ray diffraction (XRD) data were collected by a Rigaku Ultima-IV with monochromatized CuKα radiation (λ=0.154 nm).

Reference

(1) Sheik-Bahae, M., Said, A.A., Wei, T., Hagan, D.J., Van Stryland, E.W.; *IEEE J. Quantum Electron.*, **1990**, 26, 760

(2) Kamada, K., Ohta, K., Iwase, Y., Kondo, K.; *Chem. Phys. Lett.*, **2003**, 372, 386

(3) Hirakawa, S., Hasegawa, S., Inada, Y., Tanaka, Y., Kawamata, J.; *Jpn. J. Appl. Phys.*, **2007**, 46, L1203